

THESIS

IODINE COMPATIBLE HOLLOW CATHODE

Submitted by

Seth Joseph Thompson

Department of Mechanical Engineering

In partial fulfillment of the requirements

For the Degree of Master of Science

Colorado State University

Fort Collins, Colorado

Spring 2019

Master's Committee:

Advisor: John D. Williams

Co-Advisor: Casey C. Farnell

Azer P. Yalin

Jose de la Venta Granda

Copyright by Seth Joseph Thompson 2019

All Rights Reserved

## ABSTRACT

### IODINE COMPATIBLE HOLLOW CATHODE

Most electric propulsion (EP) systems utilize xenon gas as a propellant, which is expensive and must be stored in heavy high-pressure tanks, within which the storage density is still lower than desired. The halogen iodine ( $I_2$ ) has risen as a leading alternative propellant with the potential to overcome these drawbacks with its lower cost, higher storage density, and significantly reduced tank pressure. Hall-effect thrusters have been operated with iodine propellant in the range of a hundreds of watts to greater than ten kilowatts [1], [2], with performance comparable to that of devices operated on xenon; however, due to the reactive nature of iodine, the hollow cathode electron sources used with these thrusters, have been operated on xenon. Without being able to operate cathodes on iodine, the consideration of iodine propellant for many space missions is not possible. This research aims to develop and examine hollow cathode assemblies capable of operating on iodine propellant. We propose that a cathode can be constructed with iodine resistant materials and with an insert capable of participating in a tungsten-iodine life cycle that is utilized in halogen lamps to increase filament lifetime. Results from this work demonstrate that a cathode with a graphite tube and a tungsten-based ceramic-metal composite insert is capable of being operated on iodine for longer than any currently published operation time. This type of cathode has the potential to be operated on iodine for over 3,000 hours, a lifetime approaching the minimum requirement of EP systems currently being used.

## ACKNOWLEDGEMENTS

The research conducted in this thesis would not have been possible without the financial backing of the NASA - SBIR Program, Contract: NNX17CC71P.

I would first like to thank my advisor, Professor John D. Williams, for his consistent guidance and support throughout this research project. His willingness to share his expertise and innovative ideas were crucial to overcoming the challenges faced throughout this research. I would next like to thank my co-advisor, Dr. Casey C. Farnell, for his direct support of all research presented in this thesis, and in particular his invaluable formulation of the research topic and methodology. I would also like to thank my other committee members, Dr. Azer P. Yalin and Dr. Jose de la Venta, for their support and guidance in the formation and presentation of this thesis.

I would also like to thank members from the CSU CEPPE Lab for their efforts related to this research presented here. I would like to thank Tucker Hensen for his considerable effort in the commissioning of the CSU based iodine test facilities, work on the iodine reaction model, and his assistance in SEM imaging. I would also like to thank Desiree Williams and Dr. John P. Chandler for their efforts related to SEM and EDS imaging. I would also like to thank Desiree for her considerable organizational efforts, without which, this thesis may never have come into existence. Finally, I would like to thank the continued support from the other lab members Cody Farnell, Jack VanGemert, Shawn Farnell, and Ryan Ham, whose direct efforts have enabled future research in this area.

Lastly, I would like to thank my family and friends for their counsel and support throughout this research. I would not have made it through without any of them.

## TABLE OF CONTENTS

ABSTRACT .....	ii
ACKNOWLEDGEMENTS.....	iii
1 Introduction.....	1
1.1 Electric Propulsion.....	1
1.2 Hollow Cathodes.....	3
1.2.1 Hollow Cathodes.....	4
1.2.2 Low-Work-Function Inserts.....	7
1.3 Alternative Propellants in Electric Propulsion.....	9
1.3.1 Iodine compatibility issues.....	12
1.4 Proposed Iodine Compatible Hollow Cathode.....	14
1.5 Thesis Outline.....	16
2 Experimental Setup and Analysis Tools.....	17
2.1 Test Facilities.....	17
2.2 Iodine feed system.....	19
2.3 Electrical Configuration.....	22
2.4 Testing Procedure and Cathode Monitoring.....	23
2.5 SEM and EDS Analysis.....	26
3 Iodine Reaction Model.....	30
3.1 Methodology.....	30
3.2 Generalized Model Results and Discussion.....	33
4 Test Results.....	36
4.1 Cathodes Tested.....	37
4.2 Operating parameters.....	38
4.3 Post Analysis.....	41
5 Conclusion and Future Work.....	51
5.1 Conclusion.....	51
5.2 Future Work.....	53
References.....	55

# **1 Introduction**

The goal of this research is to develop and examine hollow cathode electron sources compatible for use with iodine propellant. Hollow cathodes are used in many electric propulsion (EP) devices, and their compatibility with reactive elements such as iodine would enable a host of space missions. Most significantly, in the near term, would be the enabling of cost-effective propulsion schemes for small-satellites, as well as ambitious space missions requiring large amounts of propellant that could be collected in-situ during a mission. There are also immediate gains that iodine propellant would offer to current EP devices being used, having far-reaching benefits that span from spacecraft design advantages to enhanced mission capabilities.

To understand the need for iodine compatible hollow cathodes, several introductory topics must be presented. These topics include a brief overview of electric propulsion devices applicable for use with iodine, hollow cathodes and the role they play in EP devices, and the need for alternative propellants in EP devices. This section provides a brief overview of each topic and its relevance to the topic of the thesis and concludes with an outline for the rest of the thesis.

## **1.1 Electric Propulsion**

All propulsion devices have a common goal of producing thrust to propel a spacecraft; however, EP is specifically aimed at doing so while providing high specific impulse. Three key performance parameters that are often considered when evaluating propulsion devices– thrust, specific impulse, and efficiency. While terms such as thrust and efficiency are commonly understood, specific impulse is less so. Many derivations of specific impulse

and how it relates to EP thruster performance, in particular, have been summarized previously [3]–[5], but here we will present it as analogous to the widely understood term of gas mileage. As a result, it is easy to understand that thrusters with higher specific impulse require less propellant to complete any given space mission. Often EP devices produce specific impulse values that are three to ten times higher than that of chemical rockets.

Although there are many electric propulsion devices, there are two leading technologies used today ion and Hall-effect thrusters. These devices have flight histories in Russia, Japan, and the United States that span the last 40 years[6]–[8]. Both Hall and ion thrusters are considered electrostatic thrusters [3] and work by accelerating ions from a plasma discharge away from the spacecraft through the use of electric fields. Figures 1.1a and 1.1c show schematic representations of both hall and ion thrusters, respectively while 1.1b and 1.1d show photographs of the devices operating in the CSU Electric Propulsion and Plasma Engineering (CEPPE) Lab.

Both thrusters operate in a similar way, by first ionizing incoming propellant gas to form a plasma discharge containing ions, neutral atoms, and electrons, and then producing thrust by electrostatically accelerating the ions. The ionization of the propellant gas occurs through electron bombardment, where electrons with sufficient energy collide with a neutral gas particle to form an electron-ion pair. In the space propulsion devices discussed, some bombarding electrons and all ion beam neutralizing electrons come from a hollow cathode electron source.

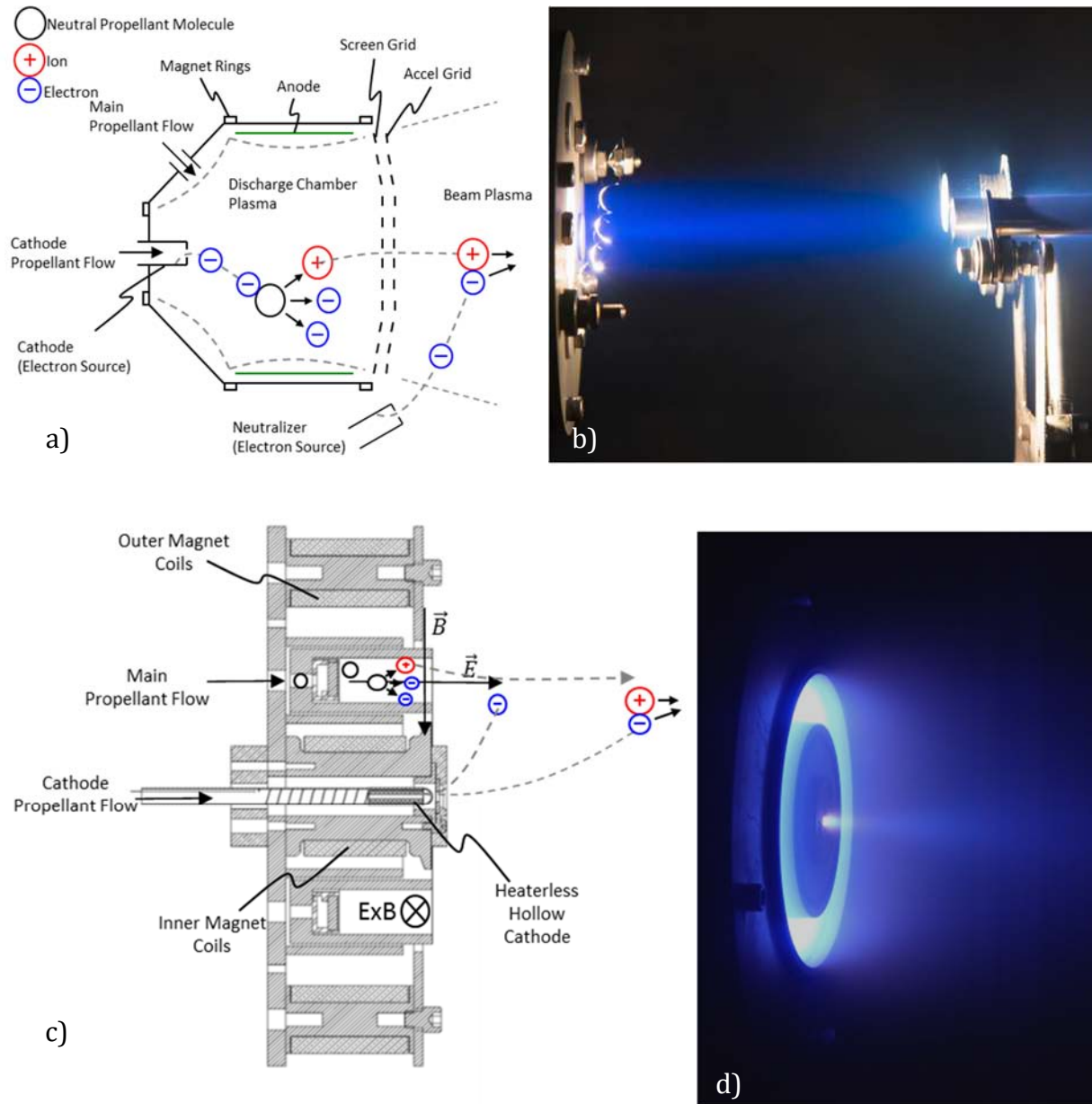


Figure 1.1: a) Schematic representation of an ion thruster b) Ion source operated at CSU c) Schematic representation of Hall thruster d) 1.5kW Hall thruster being operated on krypton at CSU

## 1.2 Hollow Cathodes

In both Hall and ion thrusters, the ions that are created and accelerated, originate from a plasma discharge that is driven in part by an electron source known as a hollow cathode. In addition to providing electrons to seed the production of the main plasma discharge,

hollow cathodes also provide electrons to the beam of accelerated ions leaving the spacecraft to prevent charge build-up that would otherwise occur if only positively charged ions exited the thruster. The configuration of the cathode, the types of materials it utilizes, and the subsequent plasma it produces largely determine both the performance and the life of the thrusters. To understand these devices in greater detail, the components and their function will be described next.

### 1.2.1 Hollow Cathodes

Although hollow cathodes are used as plasma electron sources in many applications beyond spacecraft propulsion [9]–[13], in all of these applications, the general components and the role they play remain the same. Figure 2 shows a cross-section of a typical hollow cathode and a photograph of a cathode operating on iodine as an electron source inside a specially designed vacuum test facility at the CEPPE Lab.

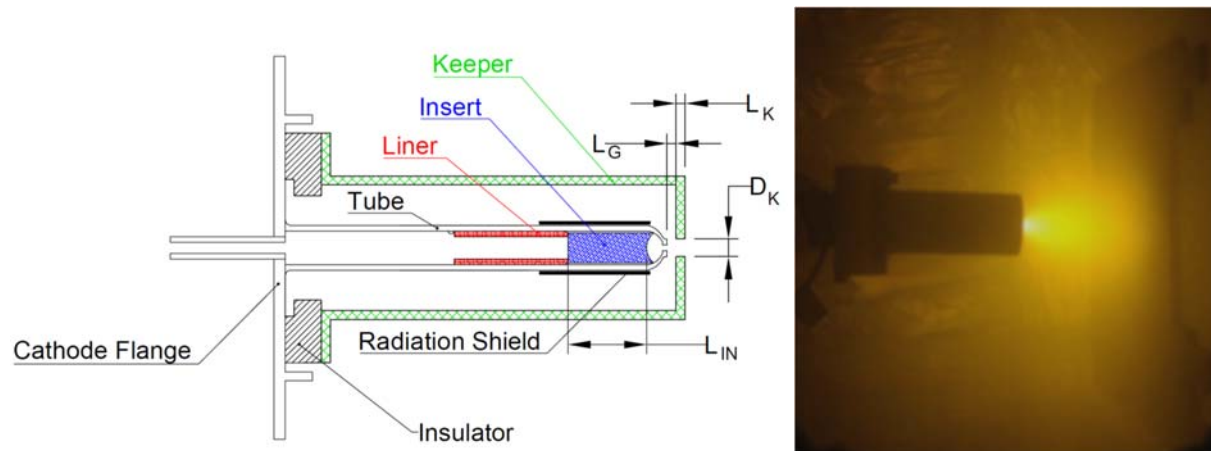


Figure 1.2: a) Cross-section of hollow cathode with components labeled b) Operation of iodine cathode as an electron source.

In the cross-section of the hollow cathode shown in figure 2a, the tube attached to the cathode flange is known as the cathode tube. This cathode tube is usually made of refractory metals like molybdenum, tungsten, or tantalum so it can withstand the high

temperatures experienced during normal cathode operation,  $\sim 1300^{\circ}\text{C}$  [14]. At the end of this tube an orifice plate is attached, usually welded, or directly formed from rolling the end of the tube, to increase the neutral gas pressure inside the tube. As the name implies, the metal tube is held at cathode potential and is in electrical contact with the insert made of electron emitting material.

Located inside the cathode tube near the orifice plate is a low-work-function insert that acts as an electron emitter. This insert thermionically emits electrons once it has been heated to a sufficiently high temperature. These electrons are accelerated away from the insert into the dense plasma, established inside the hollow cathode, giving it the energy required to heat the plasma and ionize neutral gas.

Traditionally, hollow cathodes used for electric propulsion have another component known as a heater. The heater is usually wound around the end of the cathode tube, where the radiation shield is shown in figure 2a, to heat the portion of the tube closest to the low-work-function insert. Heaters are generally a coaxial refractory metal wire with a ceramic isolator separating the center conductor from the outer sheath, which is in contact with the cathode tube [15]. These heaters are responsible for heating the cathodes to thermionic emission temperatures  $\sim 1100^{\circ}\text{C}$  through ohmic heating. Heaters require more power to operate the cathode and act as another life-limiting component on the hollow cathode, and therefore, several cathode configurations have been tested in which the cathode can be started without the use of a heater. Heaterless cathode starting has been demonstrated in a number of cathode tube and insert material configurations, and are commonly referred to as heaterless hollow cathodes [16]. Cathodes that are started without the use of a heater utilize a higher voltage and higher flow rates to initiate a Paschen breakdown and an arc

discharge with the subsequent ion bombardment onto the cathode surface heating the cathode to thermionic emission temperatures.

An additional component that can be considered part of the hollow cathode assembly is the keeper, although it is not held at cathode potential. The keeper is an electrode that can either completely enclose the cathode tube, as in figure 2a, or simply be suspended downstream of the cathode orifice. The enclosed keeper has the added benefit of confining neutral gas particles to increase the neutral density near the cathode surface for easier starting. The keeper serves two purposes, it is used to start the cathode plasma discharge and to maintain or “keep” the cathode discharge ongoing in the event that the discharge to the thruster is unstable or extinguished.

The word “hollow” part in the term hollow cathode refers to the hollow cavity that exists in the cathode tube and inside the insert’s cylindrical geometry. This cavity acts to confine neutrals and enhance discharge efficiency through the “hollow cathode effect” [17]. The enhanced characteristics of the hollow cathode effect are what make them desirable electron sources for many plasma sources. Although the understanding behind the effect is somewhat debated, with some sources claiming it’s due to the trapping of electrons electrostatically, dubbing them “pendulum” electrons that travel back and forth in the cathode cavity increasing chances for ionization events [18], [19], while others claim it to be a result of the plasma structures that are formed within the confining geometry at cathode potential [11], [20]. In either case, the advantage of the hollow cavity at cathode potential is its ability to produce higher plasma densities and current densities at much lower voltages, decreasing the power input required to extract electrons.

### 1.2.2 Low-Work-Function Inserts

The insert inside of the cathode tube shown in figure 2 is responsible for dispensing barium, which lowers the work function, allowing the cathode to emit some of the electrons used to drive the plasma production and to neutralize the beam of the ions leaving the spacecraft, preventing spacecraft charging. In general, inserts are either made from or contain material that can thermionically emit electrons as the material is heated. The temperature limited current density emitted from the insert can be given by the Richardson Dushman equation [4]:

$$j = A^* T^2 \exp^{-e\phi/kT} \quad \text{Eq. 1-1}$$

Where  $A^*$  is the product of the Sommerfield constant and a term that is varied depending on the material being considered,  $T$  is the temperature of the material,  $e$  is the charge of an electron,  $k$  is Boltzmann's constant, and  $\phi$  is the work function of the material. There are additional factors that can be added to Eq. 1-1 to account for an increase in the temperature-limited current density due to the presence of strong electric fields [4]. The Eq. 1-1 indicates that for a fixed current density  $j$ , a decrease in work function would result in a lower temperature  $T$  of the material. This is to say that materials with a lower work function can more readily emit electrons at lower temperatures, which is desirable for simplifying cathode design.

Today a common cathode insert that is used in ion and Hall thrusters is the "Phillips Type S," which is formed from porous tungsten that is impregnated with an emissive mix of barium oxide (BaO), calcium oxide (CaO), and aluminum oxide (Al<sub>2</sub>O<sub>3</sub>). Table 1 shows a summary of work functions for common materials used as cathodes.

*Table 1: List of common low work function inserts and refractory metals with their associated work function.*

<i>Insert or Material</i>	<i>Work Function</i>
<i>BaO 411- Scandate [21]</i>	2.01 eV
<i>BaO 411 [21]</i>	2.08 eV
<i>LaB<sub>6</sub> [4]</i>	2.66-2.91 eV
<i>Molybdenum [22]</i>	4.2 eV
<i>Tantalum [22]</i>	4.1 eV
<i>Tungsten [22]</i>	4.55 eV

The BaO-based impregnated porous tungsten materials listed in Table 1 work by slowly evolving barium from their interior that diffuses to the surface where it joins an oxygen atom on the surface of the tungsten, dramatically lowering the work function. Lanthanum hexaboride inserts (LaB<sub>6</sub>) emit from their surfaces without the need for dispensing barium. Although LaB<sub>6</sub> inserts have higher work functions, they are still commonly used due to their low vapor pressure, even at the higher operating temperatures that occur as a result of the higher work function [23]. The low vapor pressure of LaB<sub>6</sub> at the cathode operating temperature implies that less insert material evaporates and leaves the cathode, which would limit the cathode lifetime. Both Ba-O and LaB<sub>6</sub> hollow cathodes have been shown to have tens of thousands of hours of lifetime.

The work function of the material used inside a hollow cathode can have a significant impact on the operational temperature, the relative lifetime of the cathode, and the design of the cathode and the electronics used to operate the device. Therefore, it is easy to imagine that unexpected changes to these materials or how they operate could have negative impacts on hollow cathode performance and lifetime.

### **1.3 Alternative Propellants in Electric Propulsion**

In both ion and Hall thrusters, an inert gas such as krypton or xenon is almost exclusively used as the propellant. Many factors affect the decision to use these gasses as the primary propellants for the plasma thrusters. Xenon, for example, is inert, heavy, and has a large ionization cross-section, meaning that electrons from the cathode are more likely to ionize the xenon than other gasses with smaller ionization cross sections. Krypton is inert as well but suffers performance losses due to its lower mass and lower cross-section for ionization; however, it is sometimes used over xenon due to its significantly reduced cost.

Krypton and xenon suffer from one common shortcoming, which is low storage density. Furthermore, to achieve somewhat reasonable storage densities, specialized tanks must be designed to handle highly pressurized propellant and must be capable of handling launch loads and temperature variations during the course of a mission. This increased complexity augments the cost further from what is already high propellant storage and delivery costs.

As space missions become increasingly more ambitious, thruster technology must also advance to keep up. Mission plans to the moon, near-earth asteroids (NEAs), and mars using higher power electric propulsion devices with requirements for long lifetimes have already been published [24]–[26]. Additionally, a one hundred-kilowatt, nested hall thruster has been demonstrated with encouraging performance results [27]. Currently, all missions discussed above plan to use xenon as the propellant, with requirements ranging from 100's of kilograms to upwards of 40,000 kilograms. Not only is this highly cost prohibitive based on the current price of xenon, but the missions would have a significant impact on the global availability of xenon gas. Currently, the only way to obtain xenon gas is

by freezing it out of the atmosphere where its concentration is only 0.00086%. As of 1998, the global production of xenon gas was only 30,000-40,000 kilograms annually [28], which has to be purified to the propulsion grade xenon mandated for most flight missions [4]. Leaving one to conclude that only one ambitious mission at a time could be fueled while also limiting the worldwide availability of xenon, likely leading to an increase in its market price, making its use even more irrational. Hence, it only makes logical sense to investigate alternative propellants that can be stored at much higher densities than xenon and krypton while also providing similar or enhanced performance characteristics.

*Table 2: Propellants for consideration with electric propulsion [29]–[32].*

<i>Element</i>	<i>Xenon</i>	<i>Krypton</i>	<i>Iodine</i>	<i>Bismuth</i>	<i>Mercury</i>
<i>Atomic Mass</i>	131.3	83.8	126.9	209.0	200.59
<i>First Ionization Potential (Monatomic) eV</i>	12.1	14	10.5	7.3	10.44
<i>Peak Cross Section (<math>10^{-16}cm^2</math>)</i>	4.8	3.7	6.0	8.0	6.0
<i>Storage Density (<math>gm/cm^3</math>)</i>	1.6	0.5	4.9	9.8	13.5
<i>Melting Point °C (at 1 atm)</i>	-112	-157	113.7	271	-38.4
<i>Boiling Point °C (at 1 atm)</i>	-181	-208	184.3	768	356.6

As shown in Table 2, there are several comparable propellants that could be used in place of xenon or krypton, but as with any design decision, each propellant comes with its own challenges that currently limit their use to research realms. Figure 1.3 shows the vapor pressure of various high-density propellants to be considered for electric propulsion.

Mercury has been used for several years in electric propulsion and even has an established flight history [33]. However, the toxic nature of the material limits the ground use of the element and therefore the amount of testing that is carried out. Bismuth also looks enticing but high heat input would be required to provide adequate pressure for most propellant feed systems.

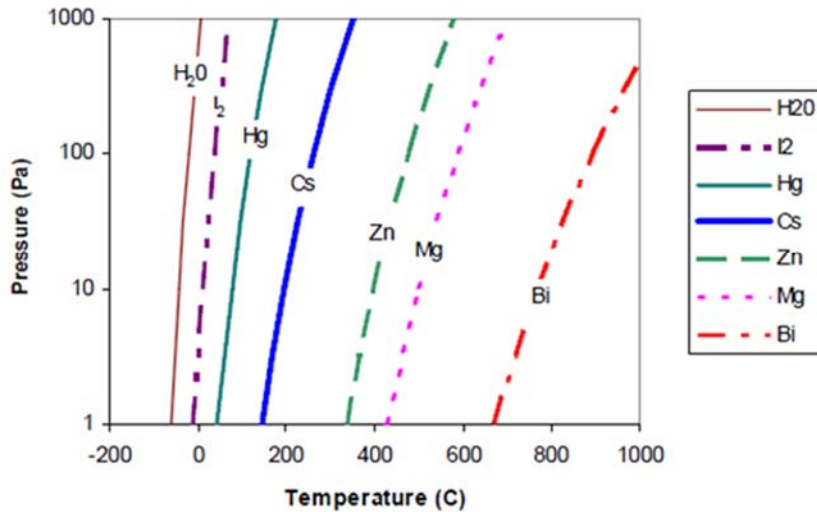


Figure 1.3: Vapor pressure curves of high density propellants taken from [34].

Although all of these propellants have been tested as possible high-storage-density alternatives to xenon [33]–[35], iodine has emerged as a clear leader amongst these options. Iodine’s storage density is over three times that of xenon and almost ten times that of krypton, with an ionization cross-section greater than both. As shown in Figure 1.3, the vapor pressure of iodine compared to that of other high-storage-density propellants is far greater at lower temperatures, making its heating system requirements much more realistic for spacecraft.

As to the abundance dilemma that plagues ambitious mission planners using xenon propellant, the worldwide production of iodine as of 1992 was 15,000,000 kilograms [36], representing roughly 375x the production of xenon. Further accolades of iodine as a potential alternative propellant are derived from the performance data that has been collected in Hall thrusters ranging from several hundred watts like the BHT-200 [2], up to ten kilowatts with the BHT-8000 [37], and performance comparable to that of xenon. The major drawback that exists for iodine is the reactivity of the halogen, which limits the lifetime of traditional cathodes to less than ~20 hours.

### 1.3.1 Iodine compatibility issues

As with any new research, it is difficult to tackle all challenges at once, and as a result of this, all prior testing of hall thrusters on iodine were done with a hollow cathode that was operated on xenon [2], [34], [37]–[39]. Iodine reacts with many of the components in a hollow cathode assembly, and especially so, at the elevated temperatures experienced during normal cathode operation. The increased reactivity of the iodine can cause undesired performance and even cathode failure. There are only a handful of published accounts of hollow cathodes being operated on iodine, but to date, no cathode has been developed to operate on iodine within the acceptable lifetimes for use in electric propulsion [34], [40].

Since iodine is a halogen of high electron affinity and not a lower affinity material, or inert gas, it tends to react more readily with materials to form compounds of iodine that typically have a high vapor pressure. This behavior can change the composition of materials or affect the geometries of components inside a hollow cathode. Table 3 shows the result of a literature review conducted for iodine reactivity with several materials suitable for cathode components at moderate temperatures below 450°C [39]. As shown in Table 3, reaction rates for these materials can be relatively small at lower temperatures but quickly rise with temperature. Although this information can serve as a guide to determine what materials may experience dramatically decreased lifetime due to exposure to iodine, the temperatures inside hollow cathode are typically much higher than 450°C.

Table 3: Data on iodine material interaction and compatibility, reproduced from [39].

REFRACTORY METAL	BASE ELEMENTS	DRY IODINE VAPOR @ 25 °C	DRY IODINE VAPOR @ 100 °C	CORROSION RATE @ 300 °C DRY IODINE VAPOR 0.53 ATM		CORROSION RATE @ 450 °C DRY IODINE VAPOR 0.53 ATM	
				mm/ year	thou/ year	mm/ year	thou/ year
<b>TUNGSTEN</b>	W	Resistant	Resistant	0	0	0.008	0.32
<b>MOLYBDENUM</b>	Mo	Resistant	Resistant	0.003	0.13	0.033	1.3
<b>TANTALUM</b>	Ta	Resistant	Resistant	0.005	0.20	0.88	35

There is little knowledge of material interactions with iodine that occur at elevated temperatures, say 1000°C to 1400°C, which is fairly typical for most cathodes. Therefore to determine what materials may be suitable in a cathode assembly, interactions at these temperatures and in the presence of dense plasma must be understood. One source of information can be found in literature from the development of halogen lamps in the 1950s and 1960s. Iodine was introduced into these lamps to increase tungsten filament life through the formation of a chemical life cycle between tungsten and iodine. As tungsten would sublime off the filament and deposit onto the bulb, the iodine vapor in the bulb would react with the deposited tungsten to form  $WI_2$  effectively scrubbing the bulb clean. The  $WI_2$  would eventually be carried back to the filament, which was operating at a temperature near 2500°C, where it would cause the  $WI_2$  compound to dissociate, depositing the tungsten back onto the filament. Molybdenum, tungsten, and platinum were often used in support structures holding the filament to avoid iodine interactions. In later years, due to the concern of iodine interactions with these support structures at elevated temperatures, graphite was substituted in these areas of elevated temperature (~1000°C) to act as an oxygen getter and to combat the water cycle that was detrimental to the lifetime of the lamps [41], [42]. We judge that research performed in the development of

these halogen lamps can act as a guide for material selection when designing a hollow cathode to be capable of operating on iodine vapor at elevated temperatures.

#### **1.4 Proposed Iodine Compatible Hollow Cathode**

As a result of the previously uncovered deleterious interactions of iodine with possible cathode materials at lower temperatures, it is expected that elevated temperatures will cause cathodes made of these materials to experience highly elevated corrosion rates along the cathode tube, insert, and other components relevant to cathode assemblies, such as the keeper and all electrical insulators. This elevated corrosion rate may cause these components to fail to perform their intended function or degrade.

Drawing from the work of halogen lamp development in the 1950s and 1960s, a cathode utilizing material such as graphite or tungsten, may have the ability to operate on iodine vapor at elevated temperatures while maintaining acceptable cathode performance for propulsion applications. As discussed previously BaO inserts are a primarily porous tungsten element that is impregnated with the low work function material. Although some of the BaO and other materials of the low work function impregnate (CaO, Al<sub>2</sub>O<sub>3</sub>, and scandium) may react with the iodine and be carried out of the cathode, the porous tungsten may participate in a tungsten-iodine chemical life cycle that would allow the insert to remain operational. Although work functions may increase closer to that of pure tungsten as the ceramic impregnate is scrubbed out, the hope is that the cathode will still operate in a stable mode at moderate voltages for the desired current densities. Furthermore, we judge that a specially designed ceramic-metal (cermet) composite could be used to enable higher temperature operation without incurring excessive performance degradation.

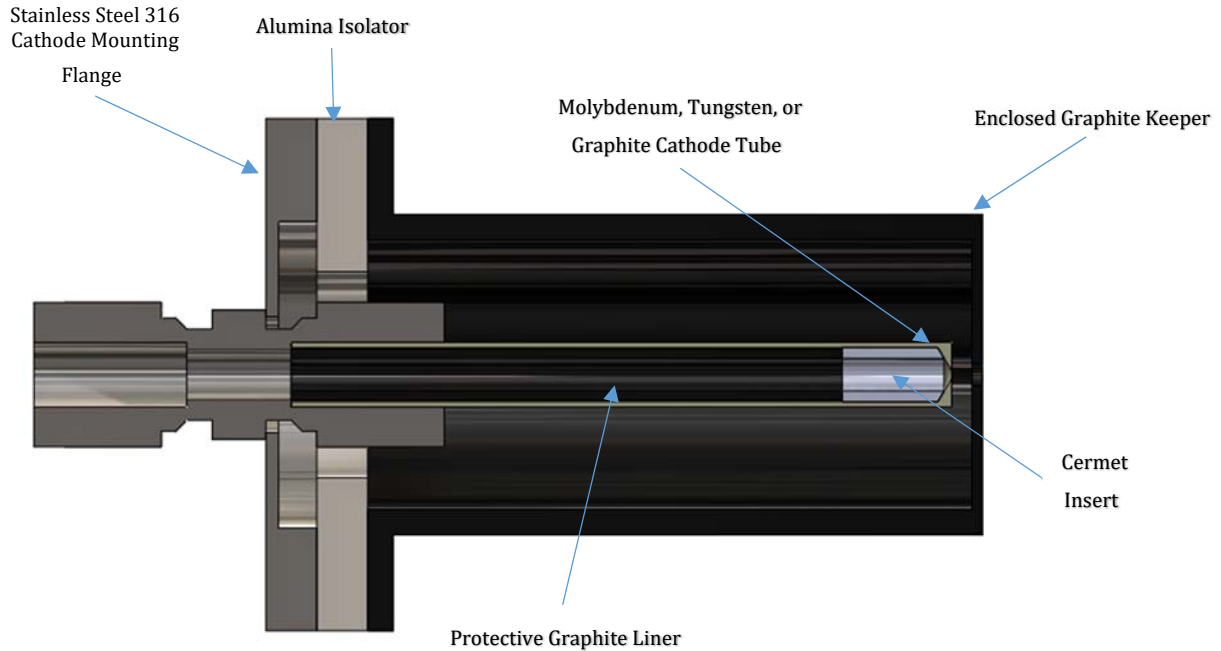


*Figure 1.4: Cross-section of iodine compatible hollow cathode*

It is proposed that a hollow cathode could be produced that utilizes materials that combat the high iodine corrosion rates and that can operate on iodine for acceptable lifetimes with acceptable performance. These cathodes would use molybdenum, tantalum, tungsten, and graphite as the cathode tube materials. Inside the cathode tube, a graphite liner would be utilized to protect the cathode tube material from the iodine avoiding increased corrosion rates, as well as to hold the specially designed insert in place. The cathode utilizes a BaO-scandate, 5-3-2-x mixture discussed in [21] and manufactured in a process described by Farnell et al. [43]. Although several changes to the insert would be expected to occur over time, the formation of a tungsten-iodine chemical life cycle with the tungsten matrix of the cermet may allow the cathode to continue to operate. **Error! Reference source not found.** shows a cross-section of a CAD model of the proposed cathode design.

## **1.5 Thesis Outline**

Chapter 2 discusses the facilities and experimental setup required to perform testing and evaluation of iodine compatible hollow cathodes, as well as the inspection tools used to perform the post-test analysis. A simplified iodine reaction model is presented in Chapter 3, with the underlying assumptions and equations specified. Results of the candidate cathodes tested on iodine, and the post-test analysis data are presented in Chapter 4. The conclusion of these results and the discussion of necessary next steps are presented in Chapter 5.

## **2 Experimental Setup and Analysis Tools**

This chapter describes how cathodes were tested and what specific aspects of their performance were measured along with the tools used to analyze the cathodes after operating them. Specifically, the following sections explain vacuum facilities, feed systems, power electronics, and inspection tools (SEM and EDS) used.

### **2.1 Test Facilities**

Hollow cathode testing is conducted under vacuum conditions to simulate the environment in which they are used with EP devices. Vacuum pumps are utilized to maintain low pressures in the cathode test facility, a process by which is complicated through the use of iodine vapor. Iodine is not only highly reactive with many materials, but iodine vapor is dangerous to humans, requiring proper containment and ventilation. Vacuum pumps utilized in testing come in contact with the iodine vapor and can be damaged due to the corrosive nature of the element. Additionally, exhaust from these pumps must be treated carefully and vented out of the facility to avoid inhalation and permanent damage to the lungs.

Early on, Colorado State University (CSU) did not have the proper facilities to perform iodine cathode testing, therefore testing was performed at two other locations, the University of Alabama Tuscaloosa (UAT) and NASA Marshall Space Flight Center (MSFC), Huntsville. Testing at UAT suffered from initial challenges related to setting up the iodine vapor feed system required for cathode testing, after which testing continued throughout the project. Testing at MSFC was performed in the interim until a suitable test facility was constructed at CSU. Figure 2.1 shows photographs of the inside and outside of the chamber

used at MSFC. The vacuum chamber used a cold trap, shown on the right, to condense iodine vapor during testing, while two 36-inch diffusion pumps were used to maintain low pressures ( $\sim 10^{-6}$  Torr). After testing, the cold trap was regenerated to increase the temperature of the surface that the iodine had condensed on, causing it to sublime and be pumped out as vapor. The vapor was then exhausted outside of the building.



*Figure 2.1: Outside (left) and inside (right) vacuum facility V7012 at MSFC used to perform iodine testing.*

The iodine-capable vacuum facility at CSU was completed after testing was performed at MSFC. Figure 2.2 shows a schematic representation and a photograph of the facility. As shown in the schematic, a cold trap, cooled with liquid nitrogen ( $\text{LN}_2$ ) was used to condense iodine vapor at a location above the diffusion pump. Similar to testing performed at MSFC, this surface was warmed after testing to sublime the iodine and pump it out of the chamber through the diffusion pump (DP) and remaining pump train. One difference between the system constructed at CSU and that of MSFC is the use of an activated carbon trap between the DP and mechanical pump (MP) in an attempt to limit the amount of iodine vapor that flows through the MP. The exhaust line for the CSU facility is also routed outside of the building like that of V7012 at MSFC to avoid exposure of humans to iodine vapor.

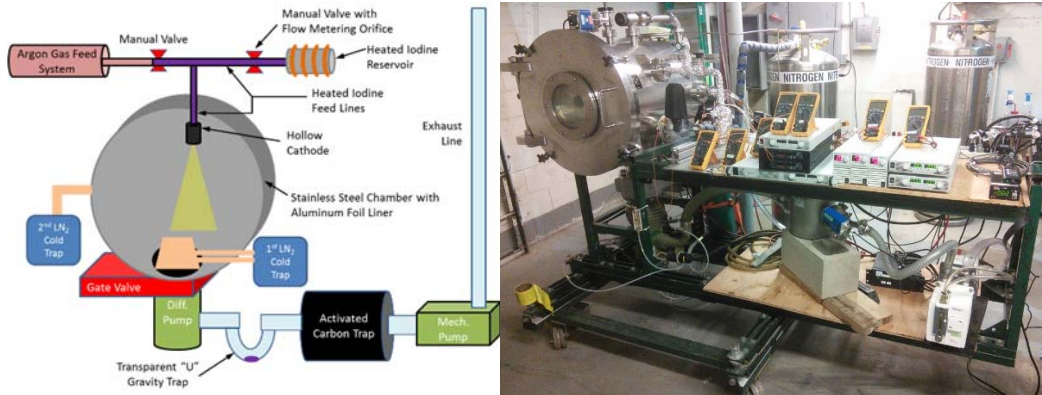


Figure 2.2: Schematic (left) and photo (right) of the CSU iodine vacuum chamber.

The CSU vacuum system utilizes a 4-inch diffusion pump to maintain vacuum and has a pumping speed of  $\sim 200$  liters per second on argon. The pumping speed of the system on iodine is higher than this because the cold trap is held at sufficiently low temperatures to pump iodine vapor cryogenically. Iodine condenses on cooler surfaces such as that of chamber walls and cold trap. The vacuum chamber is lined with sacrificial aluminum foil that reacts with the iodine vapor, protecting the stainless steel walls from corrosion. This foil is replaced after each cathode test. The condensation of iodine can lead to added complications to other components such as propellant feed systems, where clogging can occur.

## 2.2 Iodine feed system

Iodine is a condensable propellant, and unlike gaseous propellants such as xenon or krypton, it must be heated to temperatures of  $\sim 70-90^{\circ}\text{C}$  to generate sufficiently high pressure to allow a given flow rate to pass through a feed system. Since iodine vapor condenses on cooler surfaces the entire feed system, not solely the propellant reservoir, must be heated to a temperature more than the reservoir to avoid clogging. As a result, a

three-zone heating system was constructed to supply the desired iodine vapor flow rate to the cathode while maintaining sufficient feedline temperatures.

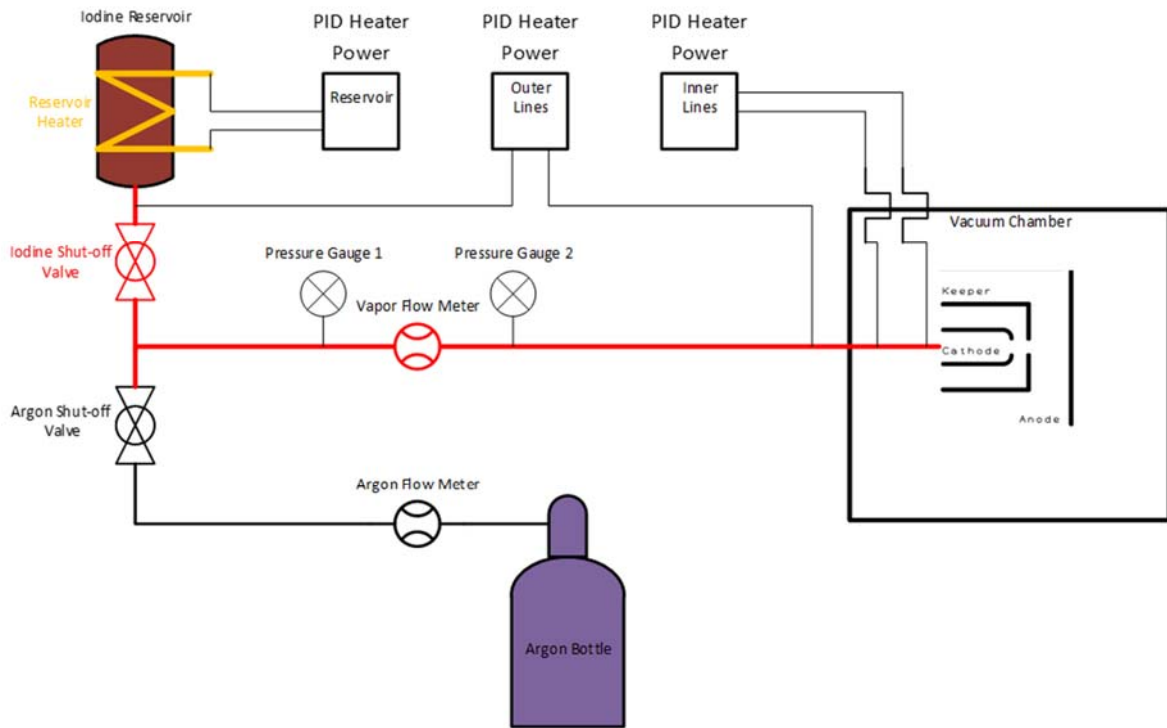


Figure 2.3: Schematic of iodine feed system for hollow cathode testing.

A schematic of the feed system is shown in **Error! Reference source not found.** Omega PID temperature controllers, utilizing type K thermocouples, were used with heaters to control the temperature of all three zones of the feed system. The iodine reservoir and outer and inner feed lines make up these three zones. The feed lines, shown in red, are held at an elevated temperature above that of the reservoir, usually near  $150^{\circ}\text{C}$ , to ensure that no condensation of iodine occurs in the feed system. The reservoir temperature was varied to set the flow rate of iodine.

The pressure inside the reservoir determines the flow rate of the iodine vapor to the cathode. The pressure is dictated by the vapor pressure of iodine, which changes with the reservoir temperature. As a result, by controlling the heat input to the reservoir and the

subsequent reservoir temperature, the flow rate of iodine vapor can be adjusted. At MSFC the flow rate was measured through the use of a vapor flow meter, containing two pressure gauges on either end of a heated tube, shown in figure 2.3, in red, in-line with the cathode. The flow rate could be calculated using the fixed viscous laminar flow equation [44]:

$$Q = k(p_1^2 - p_2^2) \quad \text{Eq. 2-1}$$

Where  $Q$  is the volumetric flow rate of iodine vapor,  $p_1$  is the pressure on the upstream end of the tube,  $p_2$  is the pressure on the downstream end of the tube, and  $k$  is a constant measured at various flow rates, described in [44]. These pressures were recorded during testing at MSFC, but no such system was implemented at the CSU test facilities. Instead, a small orifice was added in between the iodine reservoir and the feedlines, and the vapor flow was approximated for in-situ testing purposes through:

$$\dot{m} = A_{orifice} P_0 \sqrt{\frac{k}{RT} \left( \frac{2}{k+1} \right)^{\frac{k+1}{2(k-1)}}} \quad \text{Eq. 2-2}$$

Where  $A_{orifice}$  is the area of the small orifice at the exit of the reservoir,  $P_0$  is the pressure inside the iodine reservoir,  $k$  is the ratio of specific heats,  $R$  is the specific gas constant,  $T$  is the temperature of the small orifice, and  $\dot{m}$  is the mass flow rate of the iodine vapor. This equation applies the sharp-edge-orifice assumption assuming no thickness to the orifice, and assuming that the downstream pressure is sufficiently low as to maintain choked flow. As a result of these assumptions, the in-situ mass flow rate calculation is not exact but may be used to approximate flow during testing.

As evident in Eq. 2-2, if the temperature and area of the orifice are fixed then only the pressure in the reservoir can cause a change in mass flow rate. The vapor pressure of iodine can be predicted accurately, based on temperature [45], therefore, by adjusting the

heat input to the reservoir and measuring the reservoir temperature, a flow rate can be approximated and adjusted. As discussed, several factors such as pressure drop from the orifice to the cathode, inaccuracies in the measured iodine temperature, and the sharp-edge orifice assumption itself can cause errors between the actual and approximated mass flow rates. To address this, an accurate measurement of the iodine reservoir mass before and after a long-term test was used to provide a calibrated average mass flow rate for comparison to the calculated mass flow rate.

### 2.3 Electrical Configuration

The electrical scheme used to operate the hollow cathodes during testing is shown in Figure 2.4. For all testing, the cathodes were operated in triode mode, meaning that three electrodes were used, a keeper, an anode, and a cathode. Therefore, the electron current from the cathode is split to both the keeper and anode electrodes. This configuration simulates the operation of HET and ion thrusters. In testing, a conductive plate was placed downstream of the keeper orifice to serve as the anode.

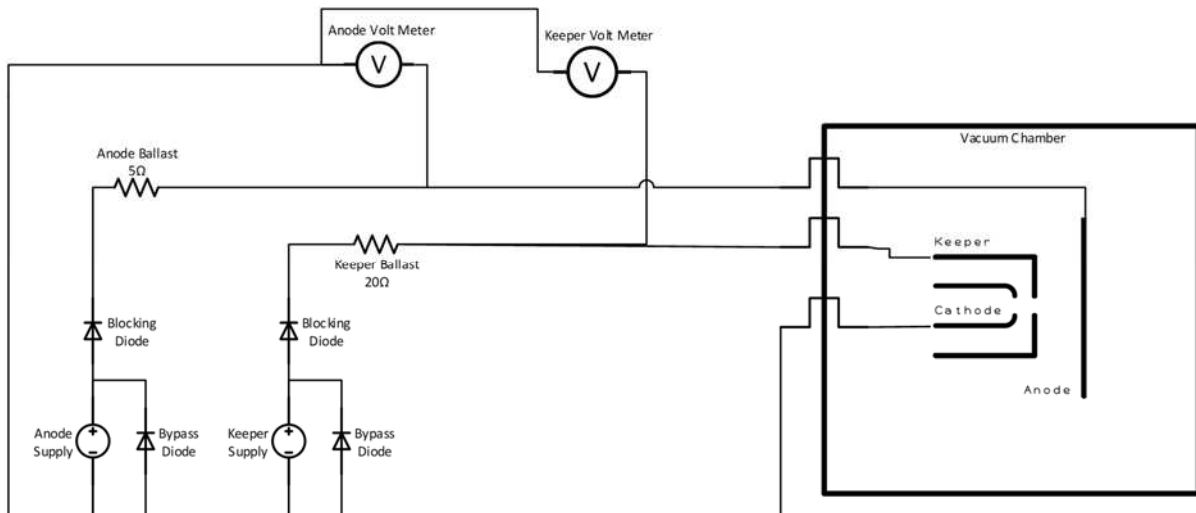


Figure 2.4: Electrical schematic used in hollow cathode testing.

The keeper power supply, used for starting and maintaining cathode operation if the anode discharge is extinguished, is a 600V, 3A DC power supply. The anode power supply, simulating the discharge power supply of a thruster, is a 100V 10A DC power supply. The bypass and blocking diodes shown in the power supply circuit were utilized to prevent damage to the power supplies in the event of difficult starts, where cathodic arcs can occur with momentary currents on the order of tens of amps[46]. Often ballast resistors are used to limit this spike in current by decreasing the available voltage to drive the discharge as the current approaches the limit set by the power supply.

#### **2.4 Testing Procedure and Cathode Monitoring**

Every cathode to be tested was installed and operated in the same manner so that a direct comparison of iodine interactions with the cathode tube and insert could be made. Each cathode tested was connected to the feedlines and electrical connectors inside the vacuum chamber. The chamber and feed lines were then pumped down to a sufficient level of vacuum ( $<10^{-5}$  Torr) before starting the cathode. The feedlines must be pumped out to avoid exposure of the cathode insert to reactive gases, like oxygen, that could damage the emitter material if present at operational temperatures. If this were to happen, it could produce observable effects that are not a result of an operation on iodine.

Heaterless hollow cathodes (HHCs) were used over traditional heater-equipped hollow cathodes, to avoid the necessity of considering the interaction between iodine and the materials used in traditional cathode heaters. By using an HHC, the focus of iodine interactions can be limited to the cathode tube and insert. Starting HHC have been shown to require higher flow rates and starting voltages than traditional heated hollow cathodes, [16], [47]–[49]. The higher voltages are required because HHCs, are started from a cold

state and must be heated to thermionic emission temperatures by a plasma discharge before nominal voltages and flow rates can be achieved. The plasma heating of the insert is initiated by a breakdown between the keeper and cathode electrodes. The voltage required to initiate this breakdown between two electrodes with neutral particle flow follows Paschen's law, where the breakdown voltage is determined by a pressure-distance product ( $p * d$ ). The distance referred to in this product is the distance between the cathode and keeper electrodes, while the pressure is that of the neutral gas or vapor in the region between the two electrodes. Initial electrons that are liberated from the cathode surface accelerate to high voltages and collide with the neutral particles. These collisions can result in ionization of the neutral particles, and the subsequent formation of electron-ion pairs. As this process continues more particles are ionized, and a plasma arc discharge is formed. The arc discharge heats the cathode surface to high temperatures through ion bombardment that results from ions accelerating toward and recombining on the negatively biased cathode surface. After the cathode tube and insert have been heated to sufficiently high temperatures (~1-3 seconds) the insert can begin to emit electrons thermionically. Subsequently, lower keeper and discharge voltages are observed, indicative of thermionic emission operation, at which point the cathode flow rate can be decreased back to nominal values.

In iodine compatible cathode testing the necessary breakdown conditions were reached by applying a high voltage between the keeper and cathode electrodes, with the use of the fixed volume release method [50] to introduce argon gas, providing a large  $pd$  product to initiate a Paschen breakdown. To accomplish this, 600V was applied to the keeper with a current limit on the keeper power supply set to 1A. The anode power supply was set to

100V with a current limit set to 5A. With no gas flow, the two supplies applied the max voltage at the electrodes in an open circuit mode. After the voltages had been applied to the electrodes, a valve was opened with a charge of neutral gas, at a pressure near that of the bottle regulator output (>1400 Torr), contained in the internal volume that exists in the feedline from the valve to the flow meter downstream of the regulator. This pressurized charge of neutral gas produces a sufficient  $pd$  product to initiate a breakdown and form a subsequent plasma arc as mentioned previously. After the gas charge was released, the cathode flow rate was maintained at a slightly elevated level until decreases in discharge voltage were observed signaling the transition to thermionic emission, when the flow was turned down to nominal levels.

Every cathode tested was first started and operated on argon gas for several minutes before shutting off argon flow and introducing iodine vapor. Initial operation on argon was done for two reasons, the first being to ensure normal operation of the cathode on a gas with which these cathodes are well characterized, confirming expected performance values before iodine testing. The second reason was to heat the cathode components to eliminate surfaces cold enough to condense iodine. If the iodine vapor was allowed to flow through any part of the cathode assembly below the feedline temperatures, flow blockages could arise as the iodine condensed. Since the focus of this research was to investigate the compatibility of the cathode tube and insert materials with iodine during steady-state operation, this starting method is sufficient; however, it would need to be examined further in later research when only iodine propellant is used.

The reactive nature of iodine, especially at higher operating temperatures, means that reactions with the cathode tube and insert material occur throughout operation. We

expected iodine to effectively scrub away the oxide-based ceramic constituents (BaO, CaO, Al<sub>2</sub>O<sub>3</sub>, and Sc<sub>2</sub>O<sub>3</sub>) from the porous tungsten matrix. The loss of the impregnate in the insert is expected cause increases in the keeper and discharge voltage of the cathode. Keeper and discharge voltages monitored throughout testing help quantify time-related effects on cathode performance, and the time required to reach steady-state operation, as the iodine reacts with the cathode tube and insert. The insert and cathode tube were both examined in an SEM to identify what changes, if any, occurred after operation on iodine.

## **2.5 SEM and EDS Analysis**

Changes to the insert and cathode tube are expected after operation on iodine. The most common tool used for identifying small surface changes and material composition of the cathode tube and insert on the relevant scales is a scanning electron microscope (SEM) equipped with energy dispersive X-ray spectroscopy (EDS) capabilities.

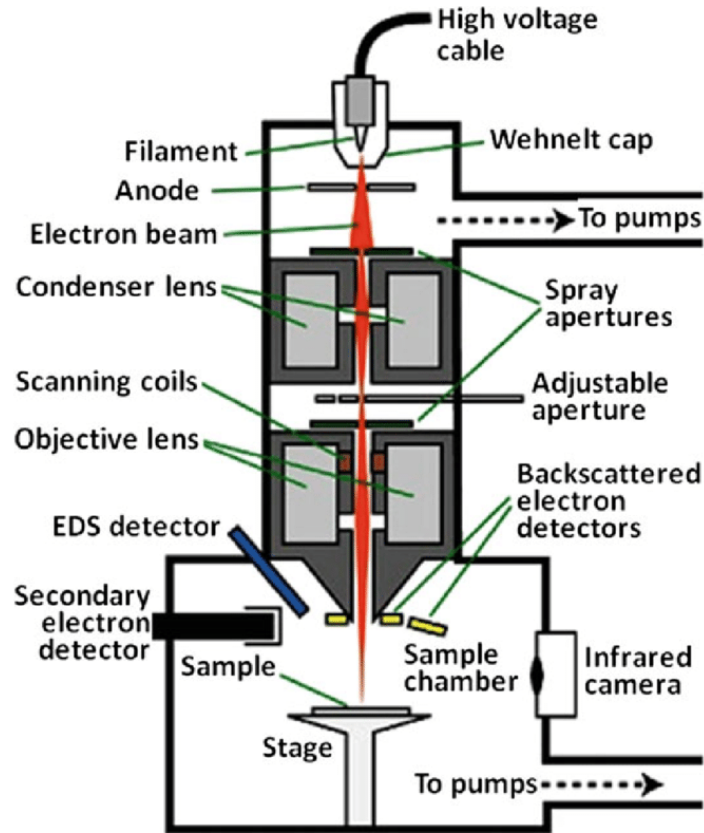


Figure 2.5: Schematic representation of a SEM with additional tools for further analysis, taken from [52].

Directly after operation of the cathodes on iodine the cathode tubes and inserts were cross-sectioned and taken to the SEM lab for analysis. The SEM uses a focused beam of high energy electrons, directed to a sample in vacuum, to cause secondary electron emission from near the surface region of the sample. Figure 2.5 shows a schematic representation of an SEM tool with additional probes for advanced analysis, that was reproduced from [51]. The secondary electrons are detected with the use of a Faraday cup, labeled as the secondary electron detector in Figure 2.5. Scanning the focused beam of electrons over the sample and monitoring the associated secondary electrons allows for images to be created with resolutions down to around 10nm [52]. In addition, the SEM can offer, through the use

of additional electron measurement techniques, an accurate topographical image of a surface.

Energy dispersive spectroscopy is a tool used in conjunction with an SEM to quantify the material composition of the samples being analyzed. The focused beam of electrons in an SEM can cause an inner shell electron to be liberated from an atom or molecule of interest, leading to an outer shell electron moving back into its place. In this process, the electron that fills the inner shell emits a photon with an energy corresponding to the difference in energy level between the two states. The EDS technique uses the difference in energy between these two electron states, which differs from atom to atom to provide elemental identification and concentration.

The photon emitted is detected by either lithium-drifted silicone (Si(Li)-EDS) or silicone drift detector designs (SDD-EDS) that provide an electronic signal from the photon that arrives at the detector. SDD-EDS is more commonly used in the past 10-15 years over Si(Li)-EDS detectors. The photoelectric absorption of the photon liberates an internal electron on the detector. This electron then has several inelastic collisions inside the detector material that produce many hole-electron pairs. The number of pairs made is directly dependent on the energy of the absorbed photon. Therefore the number of electrons that are collected can be used to indicate the energy of the photon and subsequently the type of atom or molecule struck by the incident electron beam. Determining the material composition of the insert before and after the operation of the cathodes on iodine provides the information on what changes occur at insert surface and whether or not these changes are detrimental to the inserts performance or lifetime. The use of the SEM on the cathode tubes themselves can also provide an accurate measure of

the rate of corrosion that can occur on the tube. From this measurement, a corrosion rate can be determined and be used for the validation and calibration of iodine reaction models of the cathode tube.

## 3 Iodine Reaction Model

### 3.1 Methodology

The reactive nature of iodine leads to significant corrosion of traditional cathode tube wall materials, which limits lifetime. The failure mechanism caused by this corrosion is either (a) the formation of iodides with the cathode tube wall material that are transported elsewhere, decreasing the thickness until a hole is present or (b) the blockage of iodine flow due to material build-up as these iodides are dissociated and material is re-deposited at higher temperature locations. A simplified iodine reaction model was created to estimate the corrosion rate of the cathode tube wall. The predictions of this model will be compared against results from cathode testing once these data exist. This model, once calibrated, might be used in place of cumbersome life tests, to evaluate more quickly the use of different cathode tube materials. The reaction rate of iodides forming with the tube wall material is primarily affected by temperature, cathode flow rate, and cathode tube and orifice geometry.

The temperature along the cathode tube varies with distance. A typical temperature distribution is shown in Figure 3.1 along with an assumed corrosion rate is superimposed, following the notion that increased temperature results in increased corrosion until a threshold temperature is reached where iodides are unlikely to be formed with the cathode tube material.

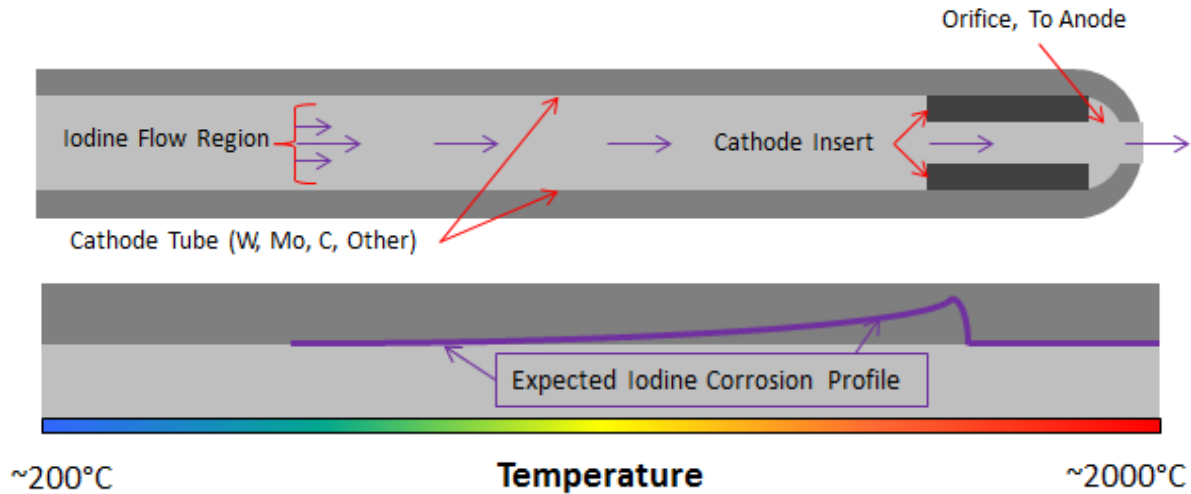


*Figure 3.1: Simplified cathode geometry (top) with hypothesized temperature and corrosion profiles (bottom) for simplified cathode geometry.*

The corrosion model developed herein relies on three base assumptions. The first assumption is that at any given temperature only the most thermodynamically favorable iodide will form. Second, it is assumed that the energy released or required for the formation of an iodide has a negligible effect on the temperature along the tube. Finally, the model does not take into account the decomposition of iodides once formed as this would result in a significantly more complex model, which would need to account for changes in cathode tube geometry due to mass transport, deposition, and decomposition kinetics in plasmas. In lieu of this complexity, it is assumed that the iodides formed are liberated from the cathode tube surface and are carried downstream through the orifice. These assumptions are supported by both the qualitative and quantitative results in the literature regarding the use of iodine in the purification of metals and the halogen lamp industry [53]. With these assumptions established the following equations that govern corrosion were formulated.

To establish the operating conditions experienced by the cathode tube during operation the pressure of iodine vapor flow must be determined. If the flow is choked through the orifice of the cathode tube and the mass flow rate is known, from pre and post-test mass measurements of the iodine reservoir, then the pressure of iodine in the cathode tube can be calculated by rearranging Eq. 2-2 as:

$$P_0 = \frac{\dot{m}}{A_{orifice} \sqrt{\frac{k}{RT} \left(\frac{2}{k+1}\right)^{\frac{k+1}{2(k-1)}}}} \quad \text{Eq. 3-1}$$

In Eq. 3-1 all of the values are the same as in Eq. 2-2, but with  $T$  and  $A_{orifice}$  now representing the temperature and area of the cathode orifice, with the other terms defined in Chapter 2. Once the pressure of the iodine in the tube is known, the density of the iodine molecules can be determined using:

$$n_{I_2} = P_0/kT \quad \text{Eq. 3-2}$$

Where  $n_i$  represents the density of the iodine molecules inside the cathode tube. If the iodine is in thermal equilibrium with the tube wall, then the random thermal is:

$$v_{th} = \sqrt{\frac{8kT}{\pi M_{I_2}}} \quad \text{Eq. 3-3}$$

In Eq. 3-3  $M_{I_2}$  is the mass of the iodine molecule. Finally, the number flux of iodine molecules approaching the cathode tube surface is:

$$\Gamma = \frac{1}{4} n_i v_{th} \quad \text{Eq. 3-4}$$

With the flux of iodine atoms ( $\Gamma$ ) to the cathode tube wall known, a corrosion rate can be determined by multiplying the probability of the formation of an iodide compound by the flux of the iodine to the cathode tube surface. This probability of reaction is given by:

$$P_{rxn} = C \exp\left(-\frac{q}{kT_w}\right) \quad \text{Eq. 3-5}$$

Where  $C$  is an empirically derived pre-exponential factor,  $Q$  is the per number reaction activation energy for the metal iodide being considered, and  $T_w$  is the temperature of the wall material. This probability takes the form of the Arrhenius relationship, with the exponential term representing the ratio of the required activation energy over that of the available energy of the wall material. As this ratio grows larger, the reaction rate will decay, but as it grows smaller, as the temperature of the wall increases, the reaction rate rises. The resulting rate of corrosion thickness (cm/s) with the tube wall equation is:

$$\dot{t}_{wall} = \Gamma P_{rxn} \left( \frac{M_M}{\rho_M} \right) \left( \frac{2}{I^*} \right) \quad \text{Eq. 3-6}$$

In Eq. 3-6  $M_M$  is the mass of an atom comprising the cathode tube material, and  $\rho_M$  is the density of that material, the ratio of the two resulting in the number of cathode material atoms per unit volume. The variable  $I^*$  is the number of required iodine atoms to form the iodide being considered. In this model, several values for variables such as reaction type, activation energy, reaction specific pre-exponential factor, and mass flow rate of iodine must first be in hand to solve for the corrosion rate. Due to the hazards inherent in working with corrosive gases like the halogens, as well as relatively limited historical applications, data for metal iodides in the desired temperature and pressure regimes is limited [54]–[56]. Full characterization of these properties could be avoided with a rough ad-hoc model that could be iteratively tuned to an acceptable level of accuracy through the post-test analysis of cathode tubes. The model could then be adjusted to fit results without the need to fully characterize iodine reactions occurring within the cathode.

### 3.2 Generalized Model Results and Discussion

Until iteratively tuned values can be derived from testing, preliminary results from the model were obtained using estimated values for activation energy ( $Q$ ), the pre-exponential

factor ( $C$ ), mass flow rate of iodine ( $\dot{m}$ ), and entropy and enthalpy of formation for the calculation of Gibbs free energy. This was done to gain insights into how a hollow cathode might erode when exposed to iodine. Example results showing a corrosion thickness after 20 hours of operation at iodine with a mass flow rate of 5 sccm  $I_2$  are presented in Figure 3.2 covering only the formation of tungsten diiodide ( $WI_2$ ), as it is the most commonly reported and most thermodynamically stable iodide formed in the tungsten system. From many sources in the halogen lamp industry, it has been reported that there is a threshold temperature above which there are no stable iodides produced. In regions above this temperature, it is expected that any iodide formation is immediately reversed and does not result in corrosion or mass transport [41], [53]. For reference, a typical cathode wall thickness is 0.38 mm, meaning the wall would be entirely eroded in just 20 hours. Although this is just qualitative analysis of the of actual reaction process, until accurate pre-exponential factors and activation energies specific for the system can be determined, the need to address corrosion of the tube wall demands more than just increased thickness.

When the model is adapted for molybdenum, erosion results are higher due to the lower density of molybdenum compared to tungsten, with the same assumptions regarding the formation of a diiodide ( $MoI_2$ ) and a similar threshold temperature for stable iodides. We note that similar estimations cannot be done assuming tubes are made from graphite as carbon-iodine compounds are not known to occur through direct reactions at any temperature [53].

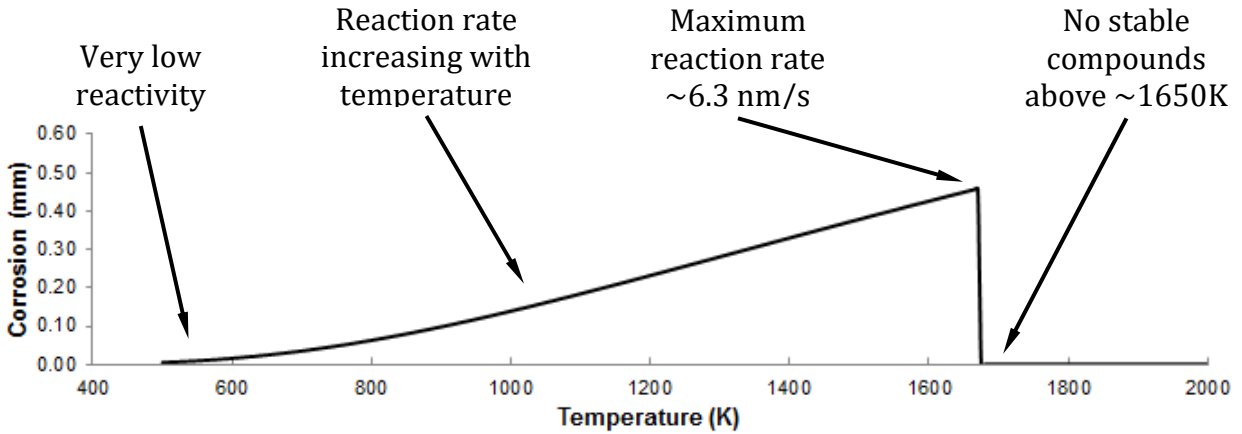


Figure 3.2: Example calculation of corrosion along tungsten cathode tube after 20 hours of operation.

Experiments reported within this thesis with graphite tubes with tungsten-based cermet inserts performed over 72 hours at an iodine flow of 0.76 mg/s support the statement that graphite is not substantially attacked by iodine. In addition, because the insert in the 72-hour test didn't display significant erosion in the downstream region near the graphite orifice, we judge that the downstream portion of the tungsten-based insert was at an adequately high temperature, where W-I reactions are not favored (though erosion may be present further upstream on the insert in cooler regions).

Further testing is required to validate the model entirely. Since the testing presented in this thesis examines either fully graphite or refractory metal cathode tubes with a graphite liner, no direct examination of cathode tube wall thickness with respect to iodine operation time was conducted with an exposed refractory metal tube.

## 4 Test Results

The goal of this project is to design and evaluate a cathode capable of operating on iodine for the purpose of use with EP thrusters. Lifetime and performance (keeper and anode voltage) are factors of primary concern for cathodes tested on iodine. The aim of testing was to measure keeper and anode voltage versus operating time and examine what changes occur in the cathode after operation on iodine.

Three vacuum facilities were used for cathode testing, and photographs of the most successful test at each location are shown in Figure 4.1. At MSFC a cathode was operated on iodine for 8.4 hours before voluntarily terminating the test. A cathode was operated on iodine for a cumulative time of ~20 hours at UAT, but several separate tests were required to achieve this operational time due to plugging of the cathode orifice. The most successful operation of a cathode on iodine was at CSU in the CEPPE Lab, where a cathode was operated on iodine for 72 hours before voluntarily terminating the test to perform destructive analysis.



*Figure 4.1: Photographs of cathodes operating on iodine at all three facilities: UA (left), MSFC (middle), CSU (right).*

#### 4.1 Cathodes Tested

As previously described, several materials were considered for use in cathodes. The insert used for electron emission and the graphite liner used to limit iodine contact with the cathode tube wall at operational temperatures, remained the same for all cathode testing, but tungsten, molybdenum, tantalum, and graphite were varied as cathode tube materials. The configuration of these cathode tube materials, their geometries, and location of testing are summarized in Table 4. The cathode tested at MSFC for 8.4 hours utilized a graphite tube. The cathode tested for 20 hours at UAT utilized a tungsten tube. The final cathode tested at CSU was also a graphite tube, which was selected after the success of testing at MSFC.

*Table 4: Summary of cathode tube configurations tested.*

<b>Cathode tube material</b>	<b>Tube diameter</b>	<b>Wall Thickness</b>	<b>Cathode orifice diameter</b>	<b>Iodine Test Location*</b>
	(inches)	(inches)	(inches)	
<b>Mo</b>	0.125	0.020	0.035	UA
<b>W</b>	0.25	0.040	0.031	UA
<b>Mo</b>	0.25	0.040	0.031	UA
<b>W</b>	0.25	0.040	0.029	UA
<b>Mo</b>	0.25	0.040	0.031	CSU
<b>Graphite</b>	0.25	0.020	0.031	MSFC
<b>W</b>	0.25	0.040	0.060	MSFC
<b>Mo</b>	0.25	0.040	0.031	MSFC
<b>Ta</b>	0.25	0.040	0.040	MSFC
<b>Ta</b>	0.25	0.040	0.040	CSU
<b>Ta</b>	0.25	0.020	0.040	UA
<b>Ta</b>	0.25	0.020	0.040	CSU
<b>Graphite</b>	0.25	0.020	0.031	CSU
<b>Graphite</b>	0.25	0.020	0.040	CSU
<b>Mo</b>	0.25	0.020	0.041	MSFC
<b>Graphite</b>	0.25	0.020	0.040	CSU
<b>W</b>	0.25	0.040	0.031	UA
<b>Graphite</b>	0.25	0.020	0.040	CSU

In general, it was observed that cathodes with refractory metal tubes suffered from plugging of the orifice that subsequently ended the tests. This process is explained in further detail in section 4.3. The material forming the plug could be removed with a drilling operation, and the cathode restarted, as was the case of the 20-hour test at UAT, but, following the drill press operation, the cathode would subsequently plug up again. Cathodes that utilized graphite tubes and orifice plates were capable of operating until voluntary terminating as was the case with the 8.4-hour and 72-hour test conducted at MSFC and CSU, respectively.

## **4.2 Operating parameters**

Orifice plugging is a failure mechanism we observed that excludes refractory metal tube and orifice plates from being considered as viable options. As a result, only the performance of tests using graphite tubes and orifice plates that were voluntarily terminated are presented here. Operation of the cathodes on iodine was expected to cause changes to the insert that may have an impact on voltage and discharge stability. More specifically, we expected that as ceramic constituents were scrubbed from the insert by the iodine plasma, the primarily tungsten material remaining would have a higher work function, which would cause the cathode to operate at higher voltages and with less stability. Relatively high voltages and an unstable discharge plasma are considered to be unacceptable cathode performance in EP thrusters. As a result, the keeper and anode discharge voltages were monitored for evidence of this process occurring. Figure 4.2 shows these voltages during operation of cathodes on iodine for test completed at MSFC.

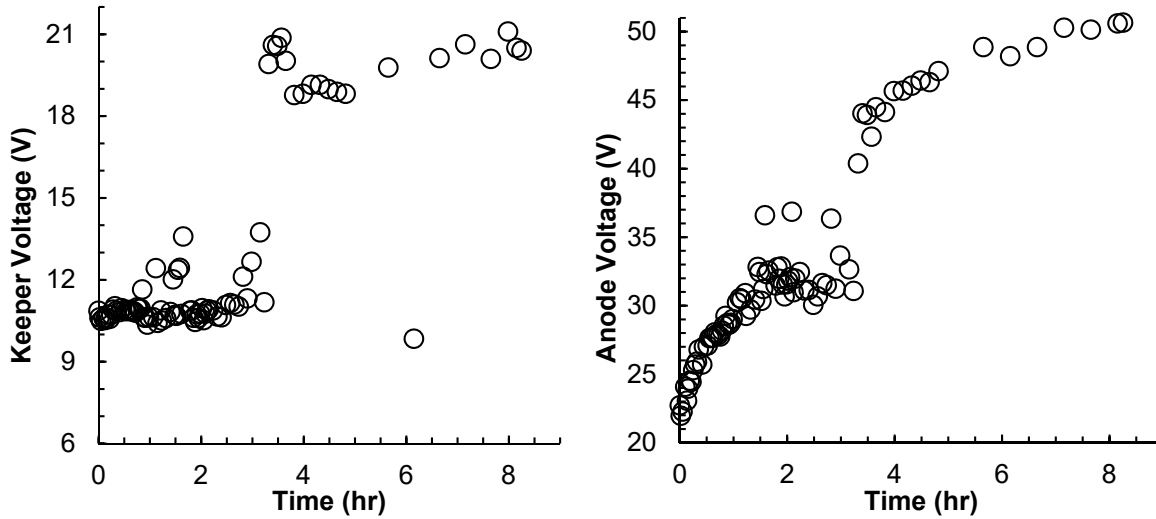


Figure 4.2: Keeper and anode voltage of cathode tested at MSFC.

The predicted increase in voltage, which can be most readily seen in the plot of keeper voltage, occurred after about 3.5 hours of operating on iodine where the voltage changed from ~11V to 20V. The anode voltage showed a similar change at 3.5 hours; however, it also steadily rose throughout the entirety of the test indicating poor coupling to the anode plate. It was discovered that the stainless-steel plate used as an anode, shown in Figure 4.1 (middle) and Figure 4.3, was partially covered with resistive a film. We believe this caused a constant increase in voltage that is not observed in the voltage of the keeper, which was made from graphite. It was decided that graphite would be used for both anode and keeper electrodes to prevent contamination.



*Figure 4.3: Iodide containing film on stainless steel anode after 8.4 four test conducted at MSFC. Film buildup over time believed to cause anode voltage to change.*

The same jump in operating voltage was also observed during a 72-hour test conducted at CSU, especially in the keeper voltage plot shown in Figure 4.4. The anode voltage increased at a steady rate for the first five hours of the test and then began to level off at ~35V where the voltage remained steady for the remainder of the test except for intermittent disruptions that occurred at hours 9, 24, and 56. These deviations in anode voltages were a result of changing the source of the liquid nitrogen for the iodine cold-trap. During these brief transitions, the cold-trap was unable to condense iodine vapor at the usual rate, resulting in increased background pressure within the vacuum chamber that caused a temporary decrease in the anode voltage.

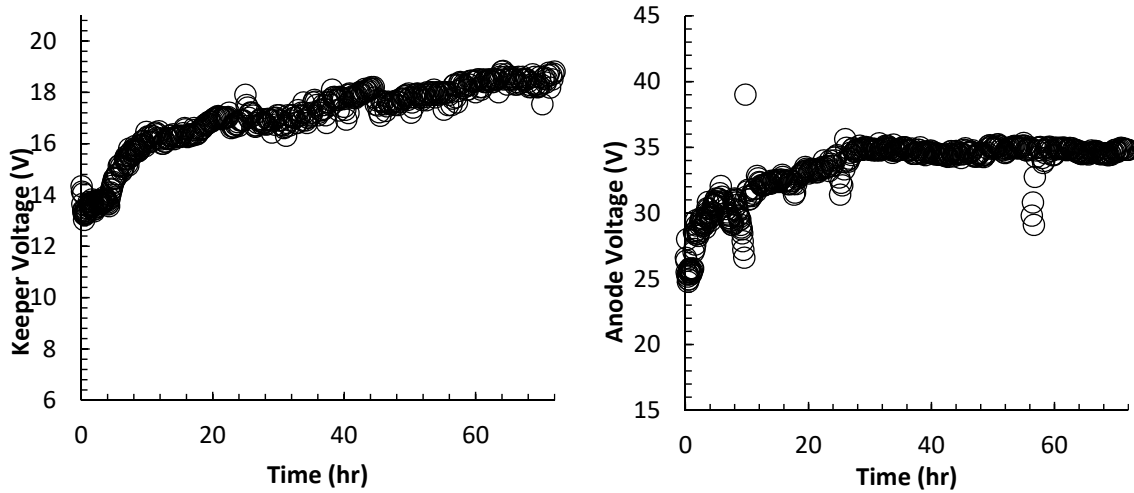


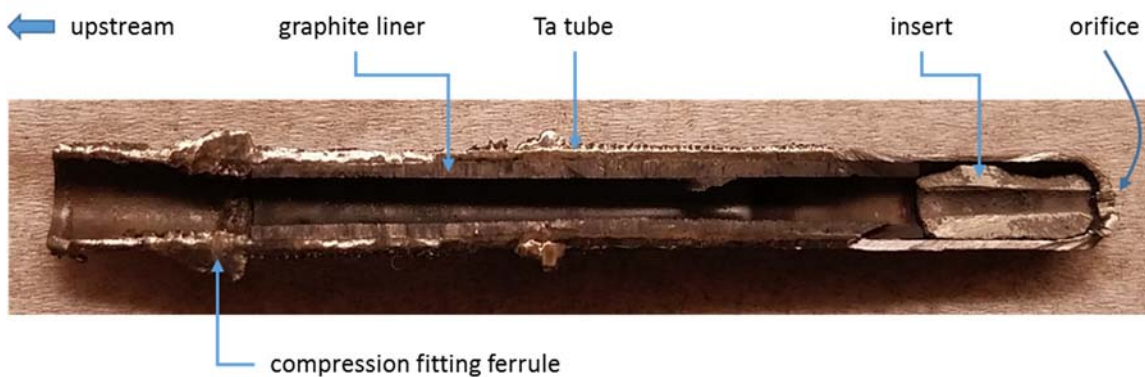
*Figure 4.4: Keeper and anode voltages of 72-hour test conducted at CSU.*

Another critical consideration in cathode operation is the mass flow rate of iodine vapor. As described in Chapter 2, the flow rate was set by controlling the reservoir temperature, which fixed the reservoir pressure. The only way to measure the flow rate accurately was from mass measurements of the iodine reservoir before and after a run. It's believed (from increased temperature measurements) that the initial flow rate of  $I_2$  was about 5 sccm, with about 4.0 sccm of  $I_2$  flowing from hours 1 through 72 (measured by the total mass change of the iodine tank before and after the 72-hour run). During hours 1-72, the average iodine flow rate was 0.76 mg/s with 8.2 A of total emission current, 5.2 A of discharge current at  $\sim 33$  V and 3.0 A of keeper current at  $\sim 16$  V. The flow rate corresponds to  $\sim 8$  % of the anode flow for a Hall Effect Thruster (HET) operated at 1.5 kW and 300V.

### 4.3 Post Analysis

After operating the cathodes on iodine, they were extracted from the cathode assembly and cross-sectioned for analysis. As mentioned previously, tests of cathodes that utilized graphite tubes and orifice plates were terminated voluntarily, while refractory metal tubes

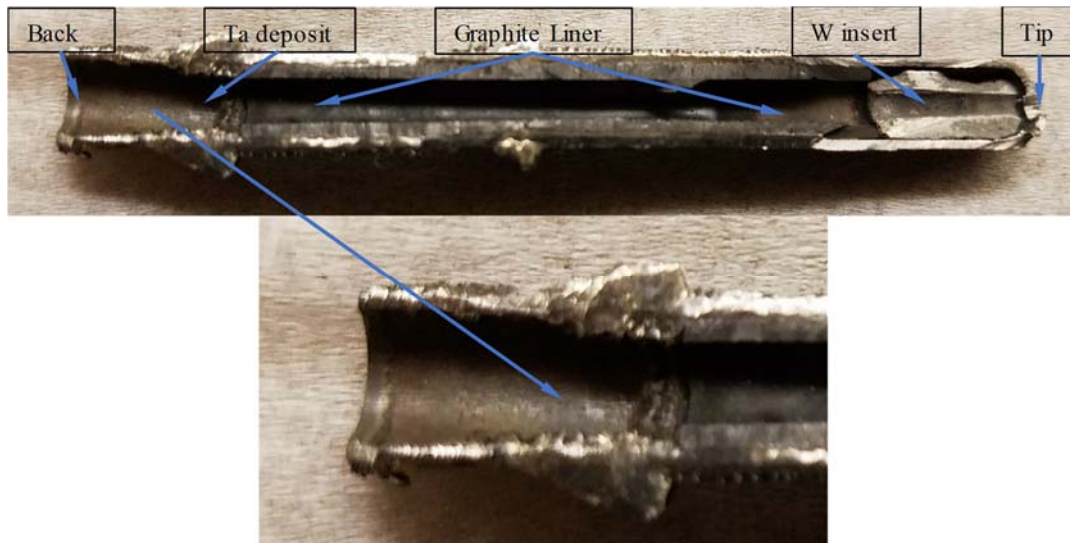
such as tantalum and molybdenum struggled with plugging of the orifice. Imaging was performed with SEM and EDS to determine the effects that operation on iodine had on the components of both graphite cathodes that were tested for 8.4 and 72 hours, respectively. Recall, that standard cathodes utilize refractory metal tubes such as tantalum or molybdenum, and that a method for addressing the increased iodine reaction rate in high-temperature regions was to insert a graphite liner to protect the cathode tube wall from iodine contact in those regions. Moreover, testing revealed cathodes utilizing refractory metal tubes suffered from fatal plugging of the orifice during operation on iodine. To examine this situation and compare it to graphite cathode analyses, one of the standard tantalum tube cathodes, utilizing a graphite liner and a cermet insert, was operated on iodine until failure (~3 hours, due to plugging), and subsequently cross-sectioned for imaging and analysis. Figure 4.5 shows a cross-section of the tantalum cathode tube, graphite liner, insert, and cathode orifice. The damage to the insert and tube was a result of cross-sectioning processes.



*Figure 4.5: Cathode tube cross-sectioned after operation on both xenon and iodine.*

Upon visual inspection of the inside, upstream region of the tube, build-up of metal tantalum deposits was observed near the compression fitting ferrule. This evidence of mass transport from the upstream region of the tube towards the downstream region. As

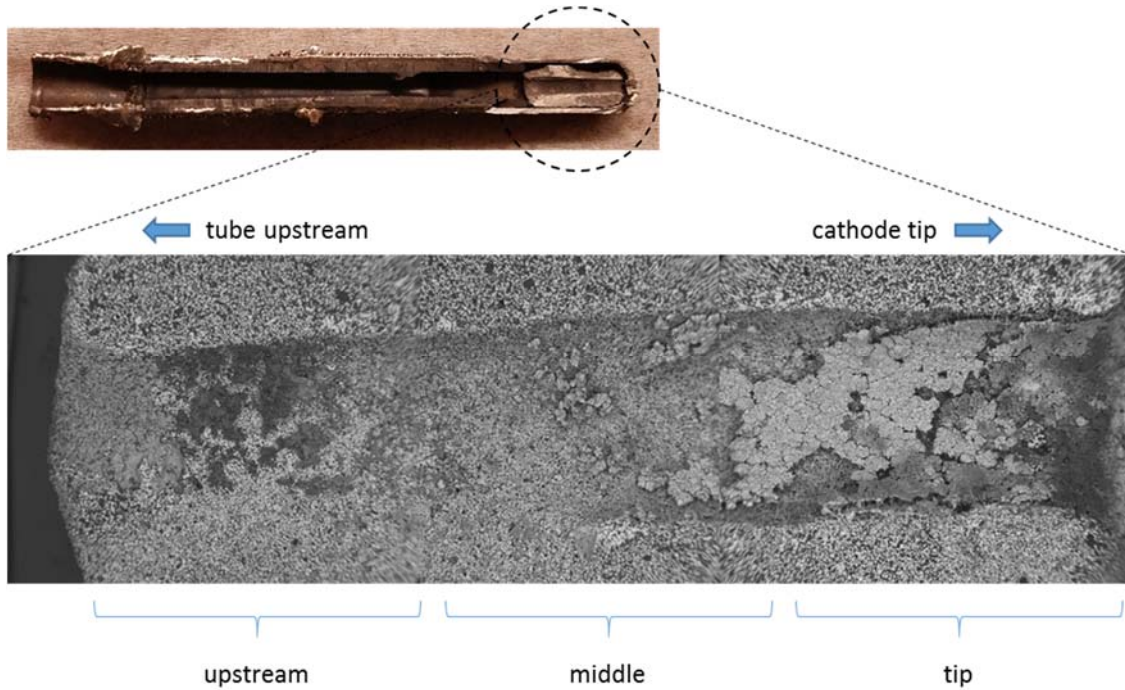
discussed in halogen lamps utilizing iodine with tungsten filaments, iodides that form at lower temperatures dissociate if exposed to sufficiently high temperatures. The corrosion model predicts a progressive thinning of the wall at upstream locations below the decomposition temperature but it does not include re-deposition processes, and, hence, does not indicate material buildup. Figure 4.6 indicates that the decomposition temperatures are achieved at the back end of the graphite sleeve, where a large tantalum deposit can be seen. Due to the relatively low decomposition temperature of tantalum iodides ( $\sim 800^{\circ}\text{C}$ ) and relatively high thermal conductivity of graphite ( $70\text{-}400\text{ W/m}\cdot\text{k}$ ) compared to tantalum ( $\sim 55\text{ W/m}\cdot\text{k}$ ), it is likely that  $800^{\circ}\text{C}$  was achieved at this point due to conduction through the graphite from the insert tip at high temperature ( $>1200^{\circ}\text{C}$ ).



*Figure 4.6: Tantalum deposit location upstream near the end of the graphite sleeve.*

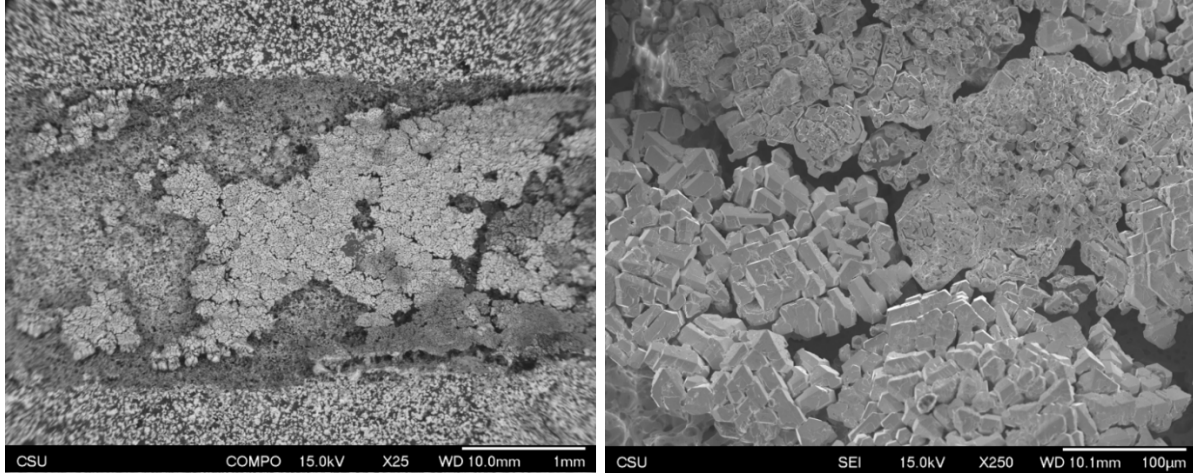
The insert was removed and selectively, mechanically dry polished in preparation for SEM viewing. Surfaces along the plane of the paper were polished, while the tubular surface along the insert's centerline was left untouched. Figure 4.7 shows three regions of the insert that were imaged: upstream, middle, and tip. Material build-up near the cathode

tip is evident, while the middles in upstream regions appear to have little to none. The middle and upstream regions are at lower temperature, supporting the notion that temperatures near the cathode tip are high enough to dissociate iodides that are formed upstream. This re-deposition process can account for the blockages observed in the testing of refractory metal cathode tubes.



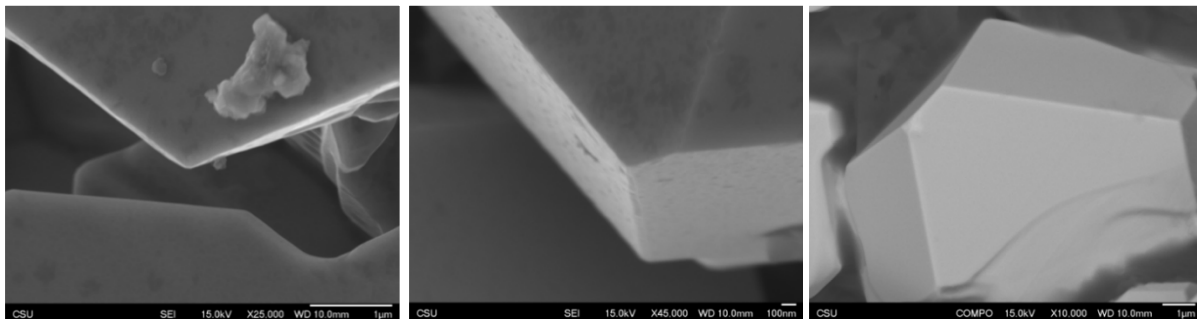
*Figure 4.7: SEM image of the insert after polishing.*

Figure 4.8 shows compositional analysis (COMPO) images of the tip region of the insert. In the COMPO-type images, light gray surfaces are tungsten, and the dark gray surfaces are ceramic. In the image on the left pure tungsten crystals were grown along the gas flow path of the insert during operation on iodine. Two discrete variations of crystals were observed as shown in the image on the right. There, crystals with very sharp edges constitute the majority along with some pyramid-shaped points. The surface of this tungsten region is largely void of ceramic; however, barium migration to the surface can still likely occur from the porous subsurface bulk material if any barium remains in these regions.



*Figure 4.8: SEM COMPO images of the insert at (left) 25x and (right) 250x magnification.*

Figure 4.9 shows zoomed in examples of the sharp-edged features of the tungsten crystals. The crystals show edges with radii of curvature  $\sim 10$  nm, which is the resolution of our SEM. We speculate that these sharp edges may act as electric field concentrators, which could initiate Fowler-Nordheim electron emission processes.



*Figure 4.9: Edges of the tungsten crystal formations along the centerline of the insert.*

Before operation, inserts that are imaged using SEM appear to be nearly fully dense. After operation on iodine, in Figure 4.10, it can be seen that surfaces without tungsten crystal growth are porous. We believe the pores are a result of the depletion of the ceramic components of the insert; however, inspection of these porous regions reveals residual ceramic inclusions, which survived operation on iodine. These inclusions appear to be composed of a calcium aluminate (roughly  $(\text{Al}_2\text{O}_3) (\text{CaO}_2)_3$ ) with a small portion of

scandium. Oxygen, aluminum, tungsten, and calcium can be observed in the phase analysis spectrum.

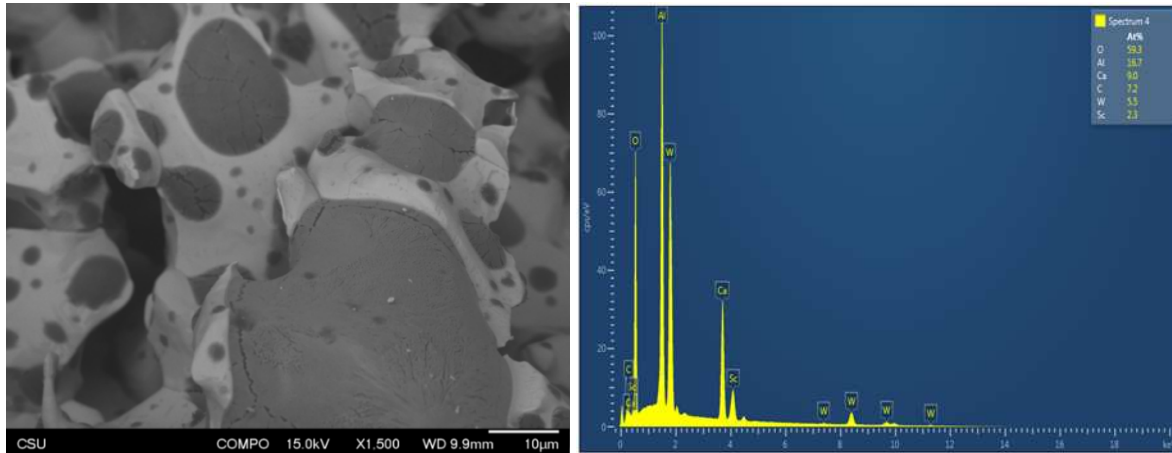


*Figure 4.10: CPMPO and phased analysis of a porous region of the insert.*

Linescans taken along the centerline plane from the upstream to the tip of the insert show a gradient in alumina concentration, with more ceramic located at the upstream side and significantly less towards the tip, until a small rise in concentration at the tip is observed. The calcium and scandium oxide concentrations were almost evenly distributed throughout.

Cathode tips that utilized a graphite tube and orifice plate were successful in operating until voluntary termination in tests that were conducted at MSFC and CSU. The graphite-based cathodes utilized the same cermet insert used in the refractory-metal-based cathodes. Cross-sections of the graphite-based cathodes from both tests were examined and the insert that operated on iodine for 72 hours was imaged with SEM and EDS.

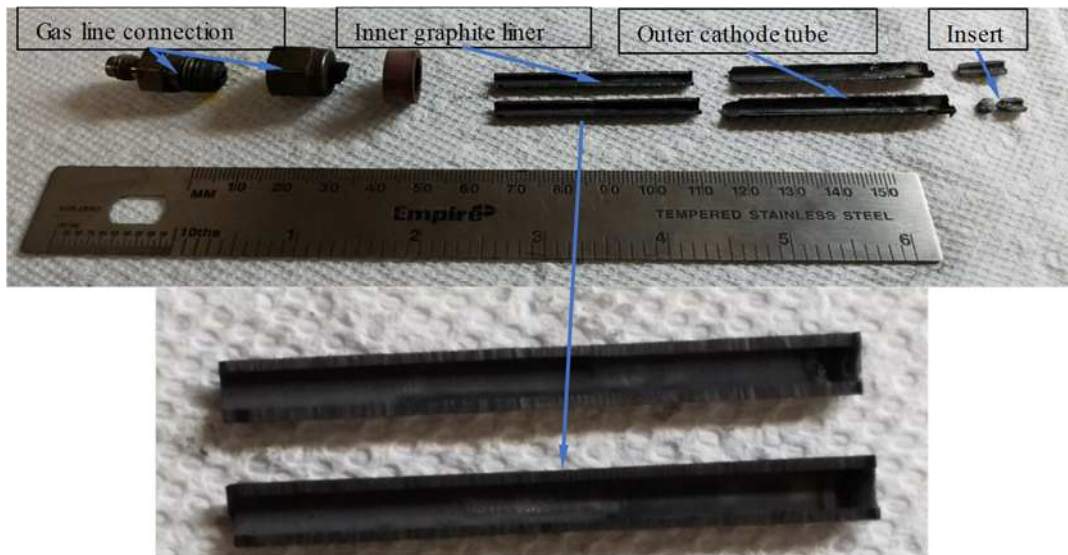


Figure 4.11: Cross-section of graphite based cathode tube and insert.

Figure 4.11 shows cross-sections of the graphite cathode tubes, inserts, inner liners, and gas connection from both tests. The top pieces being the cathode operated at MSFC and the bottom being the cathode operated at CSU. Any apparent damage to the tubes in this photo was incurred during cross-sectioning. Although rates may change slightly over time, a 72-hour test should be sufficient to demonstrate the corrosion resistance of a material for use in cathodes with extrapolation to determine expected lifetimes, with the requirement that lifetimes be >1000 hours.

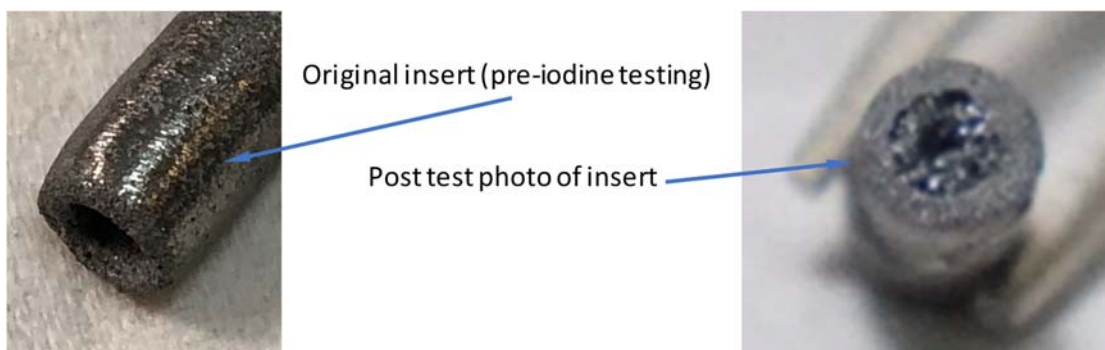
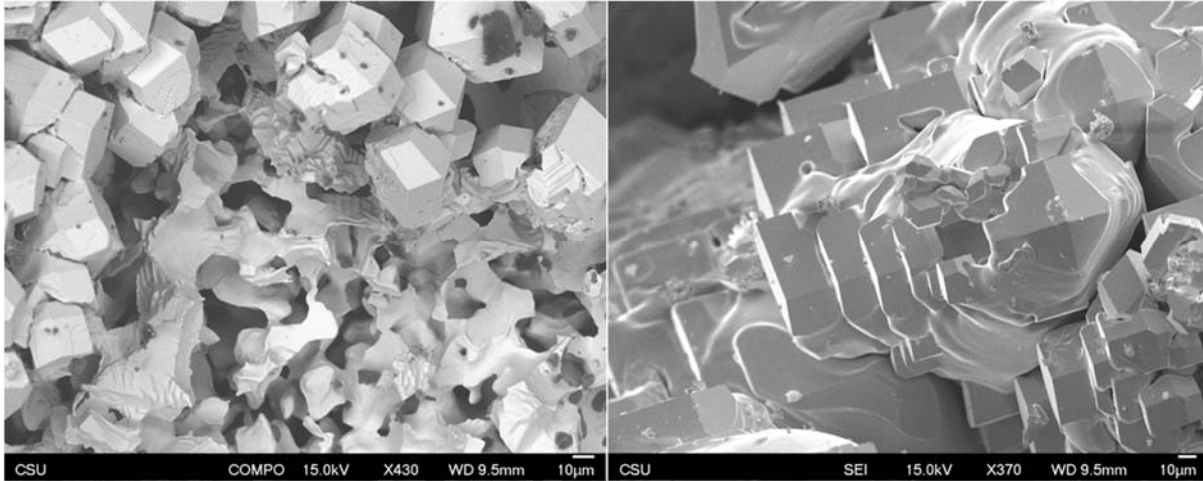


Figure 4.12: Photographs of the tubular insert pre- (left) and post- (right) iodine operation.

Examination of the graphite components after the 72-hour test showed that corrosion of the graphite cathode tube and liner were negligible as expected. The most noticeable changes due to operation on iodine were in the insert. The growth of sharp edge crystals inside the insert upstream of the orifice was visible to the naked eye and are shown in Figure 4.12. The post-test insert, shown on the right, does have visible unobstructed flow path visible near the centerline of the insert when held to the light. The original insert shows a noticeable gap in the centerline of the tubular insert that appears to have been filled, in part, by the growth of tungsten crystals.



*Figure 4.13: Pre and post operation SEM images of the insert showing tungsten-crystal growth in block-like formations over the porous tungsten matrix near the cathode orifice.*

The insert was cross-sectioned and mechanically dry polished while the surface in the center of the insert remained untouched for imaging. Figure 4.13 shows SEM images of the tungsten crystals that have grown in block-like formations with sharp edges as was observed in the previously discussed insert. EDS was used to determine if any ceramic material remained in the insert after 72-hours of operation on iodine. There were residual ceramic inclusions that appeared to have a similar composition (calcium-aluminate), to the insert previously analyzed. Figure 4.14 shows EDS measurements taken to determine the

composition of one of these inclusions found during SEM imaging. The residual ceramic in both cases show the remnants of  $Al_2O_3$  the original barium calcium aluminate ceramic mixture used to form the cermet.

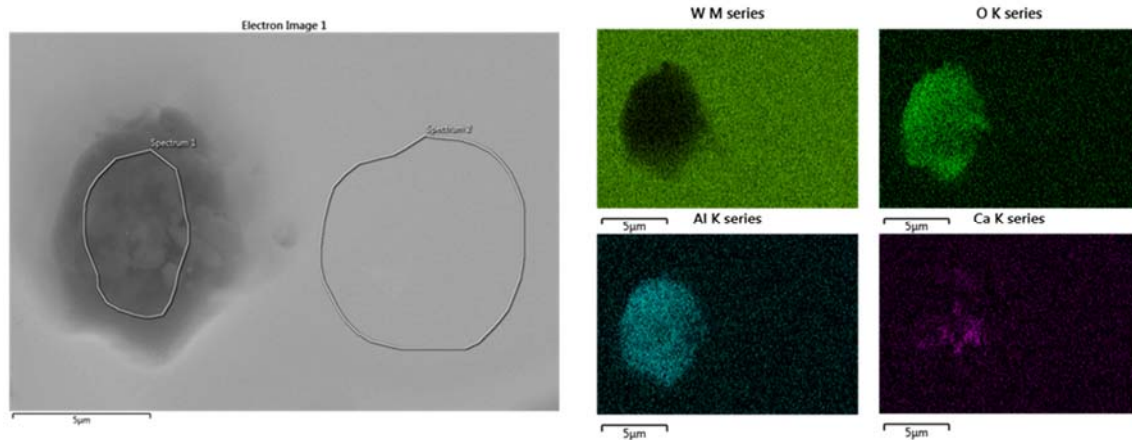


*Figure 4.14: EDS SEM scan for components on the surfaces of the post 72-hour iodine run, insert. The lighter grey surface is tungsten, while the darker area on the left of the SEM image displays aluminum, calcium, and oxygen signatures.*

Relevant to the consideration of cathode lifetime is the corrosion rate of cathode tube components in contact with iodine, especially in high-temperature regions. As was seen in examination of the tantalum cathode tube, not only was mass transport a problem for thinning of tube walls, but it also caused plugging of the cathode that terminates testing well before minimum wall thickness is reached. However, as seen in the micrographs of the graphite cathode tubes after operation (Figure 4.15) there was no observable degradation of the cathode tube and liner wall in contact with iodine and iodine plasma.

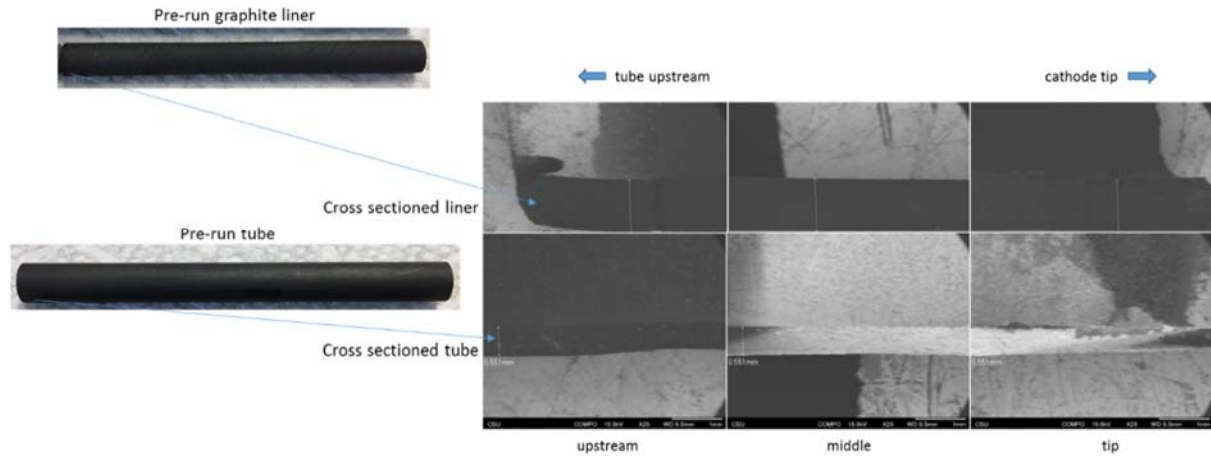


*Figure 4.15: Micrographs of the post 72-hour iodine run graphite liner and graphite tube. The pre-run liner and tube are shown for reference.*

## 5 Conclusion and Future Work

### 5.1 Conclusion

Detrimental interactions of traditional cathode components with iodine has prohibited its use as a propellant for EP thrusters even within the research realm. These detrimental interactions take the form of unacceptable corrosion and subsequent erosion rates of the cathode tubes (limiting lifetime), fast clogging of the orifice (resulting in cathode failure), and insert material transformations leading to unpredictable/decreased cathode performance. We aimed to examine possible iodine compatible cathodes that do not suffer these detrimental impacts. The means by which new cathodes were designed were based off halogen lamp work and consisted of using graphite components in high temperature areas, to avoid elevated corrosion rates, and the use of a barium-tungsten-based cermet precursor material for the insert with the potential to form a tungsten-iodine chemical cycle in the cathode tip region that would result in long lifetimes.

Testing of the proposed cathode design revealed that refractory metal tubes had increased corrosion and erosion rates, as expected, in high temperature areas, and furthermore the use of a graphite liner to protect the metal surfaces was not successful in eliminating tube corrosion. Instead, it appears that the high thermal conductivity of the graphite liner conducts sufficient heat upstream to maintain elevated temperatures there that cause increased corrosion and erosion rates in exposed metal areas normally at lower temperatures, where lower reaction rates would occur. The subsequent erosion and deposition of metals, due to dissociation of iodides formed in the metal-iodine reaction process was observed near the upstream end of the liner and around the orifice at the

downstream tip of the cathode. The deposition of the metals in these areas lead to orifice clogging that caused the flow of iodine vapor to be blocked, extinguishing the cathode discharge.

Cathode tubes made entirely of graphite did not suffer the same problems. In fact, all tests that utilized graphite cathode tubes were terminated voluntarily and did not experience orifice clogging. The longest of these tests was 72 hours, which was considered long enough to determine if any observable corrosion of the cathode tube occurred that would limit the life of the cathode. However, as shown in Figure 4.15, there was no visible degradation of the cathode tube wall after operation on iodine. As a result we recommend graphite as a top candidate material for use in iodine compatible hollow cathodes, especially in high temperature conductive, support structures that are not actively involved in thermionic electron emission.

Insert changes were expected to occur as the cathodes were operated on iodine. Reactions with the metals and ceramics in the cermet precursor material when exposed to partially ionized, iodine vapor while at high temperature has not been extensively characterized, and as such, it was difficult to predict what changes, if any, would occur to the cermet insert prior to conducting a test. Any changes causing performance degradation would exclude candidate insert material from consideration for use with iodine. As shown in Figure 4.4, although a step increase in electrode (anode and keeper) voltages after about 4 hours was observed, the performance of the cathode tested in the 72-hour run on iodine remained steady and with power levels and flow rates within the desired range for use in EP thrusters. After using an SEM with EDS to examine the insert after this test, it was discovered that little ceramic material remained within the bulk and on the surface near

the cathode tip. In addition we observed that sharp-edged tungsten crystals had formed across most of this surface. It was postulated that these sharp edges, with radii of curvature less than our SEM's resolution ( $\sim 10\text{nm}$ ), may act to concentrate electric fields and aid in electron emission. As a result of this work we conclude that, designs proposed for continued developments of iodine compatible cathodes should incorporate graphite based cathode tubes, keeper and anode electrodes, and a tungsten-based cermet insert material similar to the ones described by Farnell et al. [43].

## **5.2 Future Work**

For the continued development of iodine compatible cathodes, three aspects of the proposed design must be evaluated. The first is the lifetime of the hollow cathode when it's continually operated on iodine. The second is the ability to start and restart the cathode on iodine. The final, related evaluation task is to determine the number of cycles a cathode can be started, and restarted on iodine before cathode failure or major degradation of performance. With these three aspects of the proposed cathode design evaluated and after models of corrosion, erosion, and re-deposition are vetted, a cathode assembly could be considered for use with iodine-based EP devices already demonstrated in research labs.

To estimate the lifetime of the proposed cathode design, tests on the order of hundreds of hours must be performed. This would further confirm the lack of degradation seen in graphite-based cathode tubes to date, and allow further evaluation of the morphological changes to the insert surface over a larger time span. The insert component of the cathode has been observed to change dramatically after operation on iodine. Confirming that there is no further performance decrease after the observed voltage shift at 4 hours, is essential

in building confidence that long lifetimes can be achieved, as this would make the cathode desirable for EP systems and qualify the cermet currently used for use with iodine.

Cathodes tested in this work utilized argon to start, operate, and heat the cathode assembly before flowing iodine to avoid condensation of iodine vapor onto cold surfaces that could cause a flow-based blockage. For iodine compatible hollow cathodes to be considered for use in EP systems, the cathodes must be able to start on iodine without first operating on an inert gas. There is a need to perform testing that characterizes the necessary electronics, flow rates, and assembly heaters for starting the cathode on iodine. The cathode assembly may need to be heated externally to sufficient temperatures to flow iodine vapor through the cathode tube and insert without forming blockages. Future work will also include the development of schemes for restarting of cathodes previously operated on iodine, which we predict to be more difficult to achieve due to a lack of high secondary electron yield, dielectric material, which is removed after just a few hours of operation on iodine.

Once starting and restarting of the cathodes has been examined, a cycle test of candidate cathodes and starting circuits needs to be performed. The presence of detrimental effects from cathode starting that limit the cycle life of a candidate cathode would eliminate its potential use as an electron source for iodine-based EP systems. With these three aspects of the proposed design fully examined, iodine compatible hollow cathodes could be tested with EP thrusters already demonstrated on iodine, enabling the use of iodine as a propellant for EP devices.

## References

- [1] J. Szabo, M. Robin, S. Paintal, B. Pote, V. Hruby, and C. Freeman, "Iodine plasma propulsion test results at 1-10 kW," *IEEE Trans. Plasma Sci.*, vol. 43, no. 1, pp. 141–148, 2015.
- [2] J. Szabo *et al.*, "Performance Evaluation of an Iodine-Vapor Hall Thruster," *J. Propuls. Power*, vol. 28, no. 4, pp. 848–857, 2012.
- [3] P. J. Wilbur, R. G. Jahn, and F. C. Curran, "Space Electric Propulsion Plasmas," *IEEE Trans. Plasma Sci.*, vol. 19, no. 6, pp. 1167–1179, 1991.
- [4] D. M. Goebel and I. Katz, *Fundamentals of Electric Propulsion: Ion and Hall Thrusters*. 2008.
- [5] S. Mazouffre, "Electric propulsion for satellites and spacecraft: Established technologies and novel approaches," *Plasma Sources Science and Technology*. 2016.
- [6] V. Kim *et al.*, "Electric Propulsion Activity in Russia," *27th Int. Electr. Propuls. Conf.*, p. IEPC-01-05, 2001.
- [7] S. Shimada, K. Sato, and H. Takegahara, "20mN Class Xenon Ion Thruster for ETS -VI," in *19th AIAA/DGLR/JSASS International Electric Propulsion Conference*, 1987.
- [8] J. R. Brophy, "NASA's deep space 1 ion engine (plenary)," *Rev. Sci. Instrum.*, vol. 73, no. 2 II, p. 1071, 2002.
- [9] C. M. Horwitz, B. S. G. and M, and D. K, "Hollow cathode etching and deposition," *J. Vac. Sci. Technol. A Vacuum, Surfaces, Film.*, vol. 6, no. 3, p. 1837, 1988.
- [10] U. Helmersson, M. Lattemann, J. Bohlmark, A. P. Ehiasarian, and J. T. Gudmundsson, "Ionized physical vapor deposition (IPVD): A review of technology and applications," *Thin Solid Films*, vol. 513, no. 1–2, pp. 1–24, 2006.
- [11] S. Muhl and A. Pérez, "The use of hollow cathodes in deposition processes: A critical review," *Thin Solid Films*, vol. 579, pp. 174–198, 2015.
- [12] H. Baránková and L. Bárdoš, "Hollow cathode plasma sources for large area surface treatment," *Surf. Coatings Technol.*, vol. 146–147, pp. 486–490, 2001.
- [13] V. Burdovitsin and E. Oks, "Hollow-cathode plasma electron gun for beam generation at forepump gas pressure," *Rev. Sci. Instrum.*, vol. 70, no. 7, pp. 2975–2978, 1999.
- [14] J. E. Polk, C. M. Marrese-reading, B. Thornber, L. Dang, and L. K. Johnson, "Temperature Distributions in Hollow Cathode Emitters," in *40th*

- AIAA/ASME/SAE/ASEE Joint Propulsion Conference & Exhibit*, 2004, vol. 4116, no. July, p. AIAA 2004-4116.
- [15] T. R. Verhey, G. C. Soulas, and J. A. Mackey, "Heater Validation for the NEXT-C Hollow Cathodes," in *35th International Electric Propulsion Conference*, 2017, p. IEPC-2017-397.
- [16] D. Lev and L. Appel, "Heaterless Hollow Cathode Technology - A Critical Review," in *Space Propulsion 2016*, 2016, no. 2–6 May, pp. 1–11.
- [17] P. F. Little and A. von Engel, "The Hollow-Cathode Effect and the Theory of Glow Discharges," *Proc. R. Soc. Lond. A. Math. Phys. Sci.*, vol. 224, no. 1157, pp. 209–227, 1954.
- [18] V. I. Kolobov and L. D. Tsengin, "Analytic model of the hollow cathode effect," *Plasma Sources Sci. Technol.*, vol. 4, no. 4, pp. 551–560, 1995.
- [19] V. I. Kolobov and A. S. Metel, "Glow discharges with electrostatic confinement of fast electrons," *J. Phys. D Appl. Phys.*, vol. 48, no. 23, p. 233001, 2015.
- [20] R. R. Arslanbekov, A. A. Kudryavtsev, and R. C. Tobin, "On the hollow-cathode effect: Conventional and modified geometry," *Plasma Sources Sci. Technol.*, vol. 7, no. 3, pp. 310–322, 1998.
- [21] J. L. Cronin, "Modern Dispenser Cathodes," in *IEE Proceedings I - Solid State and Electron Devices*, 1981, vol. 128, no. 1, pp. 19–32.
- [22] W. H. Kohl, *Handbook of Materials and Techniques for Vacuum Devices*. New York, 1967.
- [23] D. M. Goebel, J. T. Crow, and A. T. Forrester, "Lanthanum hexaboride hollow cathode for dense plasma production," *Rev. Sci. Instrum.*, vol. 49, no. 4, pp. 469–472, 1978.
- [24] T. Sarver-Verhey, L. Dudzinski, T. Kerlanke, S. Oleson, and D. Hoffman, "Solar Electric Propulsion Vehicle Design Study for Cargo Transfer to Earth-Moon L1," in *38th AIAA/ASME/SAE/ASEE Joint Propulsion Conference & Exhibit*, 2002, no. November.
- [25] J. R. Brophy, R. Gershman, N. Strange, D. Landau, R. G. Merrill, and T. Kerlake, "300-kW Solar Electric Propulsion System Configuration for Human Exploration of Near-Earth Asteroids," *AIAA*, 2011.
- [26] S. N. Williams and V. Coverstone-Carroll, "Mars Missions Using Solar Electric Propulsion," *J. Spacecr. Rockets*, vol. 37, no. 1, pp. 71–77, 2000.
- [27] S. J. Hall *et al.*, "High-Power Performance of a 100-kW Class Nested Hall Thruster," in *35th International Electric Propulsion Conference, Atlanta, GA*, 2017, no. October, p.

IEPC-2017-228.

- [28] P. Haudddinger *et al.*, *Ullmann's Encyclopedia of Industrial Chemistry: Noble Gasses*, vol. 24. 2012.
- [29] D. R. Lide, Ed., *CRC Handbook of Chemistry and Physics 85th Edition*. CRC Press LLC, 2005.
- [30] J. A. Syage, "Electron-impact cross sections for multiple ionization of Kr and Xe," vol. 46, no. 9, pp. 5666–5679, 1992.
- [31] T. R. Hayes, R. C. Wetzel, and R. S. Freund, "Absolute electron-impact-ionization cross-section measurements of the halogen atoms," *Phys. Rev. A*, vol. 35, no. 2, pp. 578–584, 1987.
- [32] H. Tawara and T. Kato, "Total and Partial Ionization Cross Sections of Atoms and Ions by Electron Impact," *At. Data Nucl. Data Tables* 36, pp. 167–353, 1987.
- [33] T. Masek, "Plasma Properties and Performance of Mercury Ion Thrusters," *AIAA J.*, vol. 9, no. 2, pp. 205–212, 1971.
- [34] J. Szabo, M. Robin, S. Paintal, B. Pote, and V. Hruby, "High Density Hall Thruster Propellant Investigations," in *48th AIAA/ASME/SAE/ASEE Joint Propulsion Conference & Exhibit*, 2012, no. August, pp. 1–15.
- [35] A. Hillier *et al.*, "High Thrust Density Propellants in Hall Thrusters," in *49th AIAA/ASME/SAE/ASEE Joint Propulsion Conference*, 2011, no. AIAA Paper 2011-524, pp. 1–15.
- [36] N. N. Greenwood and A. Earnshaw, *Chemistry of the Elements*, 2nd Editio. Oxford: Reed Educational and Professional Publishing, 1984.
- [37] J. Szabo, M. Robin, S. Paintal, B. Pote, V. Hruby, and C. Freeman, "Iodine Propellant Space Propulsion," in *The 33rd International Electric Propulsion Conference*, 2013, p. 311.
- [38] J. Szabo and M. Robin, "Plasma Species Measurements in the Plume of an Iodine Fueled Hall Thruster," *J. Propuls. Power*, vol. 30, no. 5, pp. 1357–1367, 2014.
- [39] K. A. Polzin *et al.*, "Propulsion System Development for the Iodine Satellite ( iSAT ) Demonstration Mission," in *Joint Conference of 30th International Symposium on Space Technology and Science, 34th International Electric Propulsion Conference and 6th Nano-satellite Symposium*, 2015, pp. 1–14.
- [40] L. P. Rand and J. D. Williams, "Instant Start Electride Hollow Cathode," in *33rd International Electric Propulsion Conference*, 2013, pp. 1–11.
- [41] E. G. Fridrich and E. H. Wiley, "Electric Incandescent Lamp," US 3132278 A, 1964.

- [42] C. B. Collins and E. G. Zubler, "Iodine Cycle Incandescent Lamps," US 2883571 A, 1959.
- [43] C. Farnell *et al.*, "Simplified Formation Process of a Low Work Function Insert," 10,002,738 B1, 2018.
- [44] K. A. Polzin, "Iodine Hall Thruster Propellant Feed System for a CubeSat," in *50th AIAA/ASME/SAE/ASEE Joint Propulsion Conference*, 2014, pp. 1–10.
- [45] D. R. Stull, "Vapor Pressure of Pure Substances. Organic and Inorganic Compounds," *Ind. Eng. Chem.*, vol. 39, no. 4, pp. 517–540, Apr. 1947.
- [46] R. K. Ham, J. D. Williams, C. C. Farnell, S. J. Thompson, T. R. Verhey, and G. F. Benavides, "Characterization of Propellant Flow and Bias Required to Initiate an Arc Discharge in a Heaterless Hollow Cathode," in *Joint Propulsion Conference*, 2019.
- [47] R. W. Conversano *et al.*, "Development and Initial Performance Testing of a Low-Power Magnetically Shielded Hall Thruster with an Internally-Mounted Hollow Cathode," in *35th International Electric Propulsion Conference*, 2017, p. IEPC-2017-64.
- [48] V. Vekselman, Y. E. Krasik, S. Gleizer, V. T. Gurovich, A. Warshavsky, and L. Rabinovich, "Characterization of a Heaterless Hollow Cathode," *J. Propuls. Power*, vol. 29, no. 2, pp. 475–486, 2013.
- [49] A. Daykin-iliopoulos, S. Gabriel, I. Golosnoy, K. Kubota, and I. Funaki, "Investigation of Heaterless Hollow Cathode," 2015, pp. 1–9.
- [50] R. K. Ham *et al.*, "Characterization of a Fixed-Volume Release System for Initiating an Arc Discharge in a Heaterless Hollow Cathode," in *International Electric Propulsion Conference*, 2019.
- [51] C. Suryanarayana, *Aerospace Materials and Material Technologies*, no. January. 2017.
- [52] J. I. Goldstein, D. E. Newbury, J. R. Michael, N. W. M. Ritchie, J. H. J. Scott, and D. C. Joy, *Scanning Electron Microscopy and X-Ray Microanalysis*, Fourth. New York: Springer, 2018.
- [53] R. F. Rolsten, *Iodide Metals and Metal Iodides*. New York: Wiley, 1961.
- [54] J. D. Cox, D. D. Wagman, and V. A. Medvedev, "Standard Thermodynamic Properties of Chemical Substances," *J. Phys. Chem. Ref. Data J. Phys. Chem. Ref. Data Texas A M Univ. J. Phys. Chem. Ref. Data Fourth Ed.*, 1989.
- [55] K. M. Pruetz, *Chemical Resistance Guide for Metals and Alloys*. La Mesa, California: Compass Publications, 1995.
- [56] E. Rabald, *Corrosion Guide*. Londo: Elsevier Publishing Company, Inc., 1951.